

UNIVERSITY OF TWENTE.



HIDDE WIERINGA

APPLIED MATHEMATICS — UNIVERSITY OF TWENTE

MASTER THESIS

15 DECEMBER 2017

**Contact Methods for Pipelaying in a
Finite Element Framework**

Supervisors:

Dr. H. Zwart

h.j.zwart@utwente.nl

Hybrid Systems, Applied Mathematics

University of Twente

Dr.Ir. H.J.M. Geijselaers

h.j.m.geijselaers@utwente.nl

MS3, Engineering Technology

University of Twente

Submitted by:

Hidde Wieringa (s1343041)

hidde@hiddewieringa.nl

Applied Mathematics

University of Twente

Ir. F.H. De Vries

f.h.devries@utwente.nl

MS3, Engineering Technology

University of Twente

Abstract

A widely used method for sea pipelaying is the S-lay method. Simulations are run which determine the dynamics of the pipe including contact with the seabed and parts of the ship. To improve this process, a dynamic model is presented for the damped pipe. Contact is enforced using the *Penalty*, *Augmented Lagrangian* and *Augmented Barrier* methods. For these methods a *Finite Element* discretization and numerical integration steps using the *Hilber-Hughes-Taylor* method are presented.

Using an implementation of the above methods, a verification has been performed against analytical solutions. The contact methods have also been compared. For the static (equilibrium) problem, all three contact methods work well. For the dynamic problem, only the Penalty method works well. Damping with and without contact has been analyzed, as well as the dynamics of the pipe on different surface shapes.

Two simplifications have been researched. To simplify the middle section of the pipe with no contact, a transfer function can be determined which describes the behaviour of the dynamics of the pipe without calculating a numerical solution. Finally, in some situations the static solution can be used in order to determine the contact position with the seabed which simplifies the solution process further.

Contents

1 Introduction	1
1.1 Problem statement	1
2 Modelling	3
2.1 Euler-Bernoulli equations	3
2.2 Three sections of beam	5
3 Contact	7
3.1 Gap	7
3.2 Penalty method	8
3.3 Augmented Lagrangian method	8
3.4 (Augmented) Barrier method	9
3.5 Damping on contact	11
3.6 Updating rules	11
4 Analysis: Finite Element Method	15
4.1 Finite element derivation	15
4.2 Reference solution	23
5 Analysis: Simplification of middle section	25
5.1 Laplace domain	25
5.2 Approximation of transfer function	27
6 Results	31
6.1 Implementation	31
6.2 Contact	33
6.3 Integration interpolation	41
6.4 Damping	41
6.5 Shape of contact surface	43
6.6 Simplification for point of contact	44
7 Conclusion & recommendations	49
7.1 Application overview	49
7.2 Further research	50
Bibliography	53
Nomenclature	55
A Appendix	57
A.1 Hermite shape functions	57
A.2 Analytic solutions of dynamic Euler Bernoulli equation	57
A.3 Discrete Fourier Transform for eigenvalues	58
A.4 Damping on contact	59

Chapter 1

Introduction

Allseas¹ is a company that specializes in providing services for the offshore industry. One of the main tasks of Allseas is laying and protecting pipes in seas and oceans. The employed method for laying pipes is the S-lay method. The ship has a pipe factory on board, which produces a pipe from the stern (back-end) of the ship. The pipe is rolled into the water, supported by the *stinger*, a large metal construction. From there the pipe hangs almost vertically in the sea, until it reaches the seabed where it connects to the already laid pipe supported by the seabed (fig. 1.1).

In order to perform this process efficiently, safely and effectively, knowledge must be available about the behaviour of the ship, the sea, the pipe and their interactions before the actual laying of the pipe. A simulation is used to anticipate different scenarios. However, the currently used simulation software has issues in terms of performance and functionality and must be improved.

1.1 Problem statement

The aim of this research project is to construct and analyze models for the movements and dynamics of the pipe in a manner that can be computed efficiently. The pipe may be split up into multiple parts, each of which have different dynamics and behaviour depending on the contact with objects around the pipe, whether it is suspended in the sea or whether it touches the seabed. In particular the areas of the pipe where there is dynamic contact with surfaces are of interest.

A model will be created in order to model the dynamics of the pipe as well as the contact with surrounding objects in its environment. This pipe model will be used to apply contact modelling methods on. The contact methods will be analyzed for suitability, performance and stability.

Apart from the modelling of the actual dynamics of the pipe, it is also of interest to look into ways to simplify the solution process. It is interesting if it is possible to reduce (a part of) the problem such that no numerical solution of the entire pipe is required to find out information about the movements or other characteristics of the pipe. In that case, the amount of required computing power is reduced, making the simulation processes performing even better.

Research questions Concretely, this problem can be formulated into two research questions:

1. Which contact modelling methods are applicable to the pipelaying problem, compared by their performance, accuracy and stability?
2. Is it possible to simplify or predict parts of the dynamics of the pipe in order to reduce calculation times?

In the following chapters these questions will be addressed.

¹General website: <https://allseas.com/>



FIGURE 1.1: The S-lay method performed by an Allseas ship. The pipe is produced and released from the back-end of the ship, supported by the stinger. It goes downwards until it reaches the already laid pipe supported by the seabed.

Scope of project It must be noted that several things which may also be of interest to this research are out of scope for this project. During the research and in particular in the implementation of numerical methods, there may be ways to optimize and improve the supporting numerical methods. For example wider applicable Finite Element methods and improved numerical integration techniques. The analysis of the numerical theory behind these methods will not be elaborated on. Similarly, this research is not aimed at developing new numerical methods, but rather aims to apply the available methods in literature on the posed problem.

An implementation will be required in order to practically evaluate the proposed methods. The goal of the implementation is not readiness for general use but rather the ease of implementation, extensibility and visualization purposes for this research project. That means that performance or applicability to other frameworks are not of main interest, although applicability to related research is advisable.

Finally, this project looks into parts of the pipe being laid. This means that the solutions presented in the research are a detailed part of the entire pipe, rather than the entire solution of the pipe. In particular, some approximations may be made which are allowed when focussing on a small piece of pipe but cannot model the entire pipe from ship to seabed. Of course, the contact methods presented in this research must be applicable to extended models which can represent the entire pipe.

Chapter 2

Modelling

This chapter describes the modelling decisions which have been made in order to find solution methods for the pipelaying problem. First the general mathematical problem description is given. It is expanded to describe the equilibrium and to include damping. Then the contact methods are described which can be applied to model a surface where contact is enforced.

2.1 Euler-Bernoulli equations

In order to describe the movements of a pipe, a simplification is made by using the one-dimensional model for a deformable beam [1, 2, 3]. This model describes the deflection of the beam $y(t, x)$ from its resting position (a straight beam) as a function of time t and location x . It is derived as a minimization problem of the modelled energies $J_n(y)$ in the beam, which are given by

$$\min_y J_n(y) = \min_y \int_0^L \frac{1}{2} EI \left(\frac{y''}{(1 + (y')^2)^{3/2}} \right)^2 + \frac{1}{2} \mu (\dot{y})^2 - w y \, dx. \quad (2.1)$$

The constant E [N/m^2] denotes the elastic modulus which depends on the type of material the beam is made of and determines the amount of stress required to elastically deform the beam. The constant I [m^4] is the second moment of inertia and is determined by the distribution of weight in a cross-section of the beam. Finally μ [kg/m] is the mass per unit length and $w(t, x)$ [N] is the distributed load on the beam. The values of E , I and μ are assumed constant along the beam, although $w(t, x)$ does not have to be.

The first term in the integral of (2.1) describes the strain energy due to the curvature of the beam, while the second term describes the kinetic energy of the beam. The third term is the work done by the distributed load $w(t, x)$. The derivatives in the x (spatial) and t (temporal) direction are denoted with a prime ($'$) and a dot ($\dot{}$) respectively. The shape of the beam is determined by minimizing $J_n(y)$, restricted by certain boundary conditions. The domain of x is $[0, L]$ and the domain of t is $[0, \infty)$.

The boundary conditions for $x = 0$ are given by two of the four possibilities

$$y(t, 0) = \mathcal{B}_1(t) \quad y'(t, 0) = \mathcal{B}_2(t) \quad y''(t, 0) = \mathcal{B}_3(t) \quad y'''(t, 0) = \mathcal{B}_4(t), \quad (2.2)$$

and for $x = L$ by two of the four possibilities

$$y(t, L) = \mathcal{B}_5(t) \quad y'(t, L) = \mathcal{B}_6(t) \quad y''(t, L) = \mathcal{B}_7(t) \quad y'''(t, L) = \mathcal{B}_8(t). \quad (2.3)$$

The functions $\mathcal{B}_i(t)$, $i \in \{1, \dots, 8\}$ must only depend on time. Linear combinations of these boundary conditions are also possible, but are not of interest in this research. Of course, each linear combination must be non-degenerate. For example, physically it is not possible to prescribe both $y(t, 0) = 0$ (the position) and $EI y'''(t, 0) = 0$ (the shear force) at the same time. Two boundary conditions are given for $x = 0$ and two boundary conditions are given for $x = L$. This assumption can be generalized to other locations along the beam, but that is currently not of interest.

Also two initial conditions are required, given by

$$y(0, x) = y_0(x), \quad \dot{y}(0, x) = v_0(x), \quad (2.4)$$

with $y_0(x)$ and $v_0(x)$ given functions on the domain $x \in [0, L]$.

Not only the deflection y is of interest in a solution of the dynamics of the beam [2]. Also the derivative $y' \approx \theta$ which is the deflection angle. The curvature $\kappa = y''$ is closely related to the moment M (torque) in the beam, related by $EI\kappa = M$. Furthermore, taking the derivative of the moment, $M' = EI\kappa' = EIy'''$ gives the shear force in the beam. Because of these relations, the boundary conditions of the following equations may contain the constants EI for the higher-order derivatives.

2.1.1 Non-linearity

The expression in (2.1) is non-linear because of the term concerning the curvature of the beam. For deflections with small angles ($|y'| \ll 1$), the length of a piece of the beam is practically constant and thus the energy in the beam due to the curvature as given in (2.1) can be approximated by

$$EI \left(\frac{y''}{(1 + (y')^2)^{3/2}} \right)^2 \approx EI(y'')^2. \quad (2.5)$$

This substitution makes the expression for $J_n(y)$ linear. Then the minimization problem becomes

$$\min_y J(y) = \min_y \int_0^L \frac{1}{2} EI(y'')^2 + \frac{1}{2} \mu(\dot{y})^2 - wy \, dx, \quad (2.6)$$

subject to the same boundary and initial conditions as (2.1).

In [1], a valuable discussion is provided on the possibilities for analyzing and solving the non-linear form. However, the authors also note that in many applications the assumption of a small angle of deflection is valid. For the application of a hanging pipe in the sea the assumption may not be valid because parts of the beam may hang almost vertically (i.e. y' is large). This means that for this research only sections of the pipe will be analyzed for which the linear model is valid (small angles of deflection). Other methods have to be used to consider the solution for the deflection of the pipe. We refer to Chapter 4 for a small discussion of the Finite Element choices for a situation with large deflections.

2.1.2 Minimization

The expression in (2.6) is minimized in order to find the deflection $y(t, x)$. This is done using the Theorem of Euler-Lagrange [4] which allows solving the minimization problem

$$\min_y \int_0^L \mathcal{L}(t, x, y, \dot{y}, y', \ddot{y}, y'') \, dx \quad (2.7)$$

by solving the equation

$$\frac{\partial \mathcal{L}}{\partial y} - \frac{\partial}{\partial t} \frac{\partial \mathcal{L}}{\partial \dot{y}} - \frac{\partial}{\partial x} \frac{\partial \mathcal{L}}{\partial y'} + \frac{\partial^2}{\partial t^2} \frac{\partial \mathcal{L}}{\partial \ddot{y}} + \frac{\partial^2}{\partial t \partial x} \frac{\partial \mathcal{L}}{\partial \dot{y} \partial y'} + \frac{\partial^2}{\partial x^2} \frac{\partial \mathcal{L}}{\partial y''} = 0. \quad (2.8)$$

The integral minimization problem in (2.6), with \mathcal{L} the integrand of $J(y)$, can now be solved by finding a solution of the partial differential equation given by

$$EIy'''' + \mu\ddot{y} = w, \quad (2.9)$$

restricted by the same boundary conditions as (2.1). This equation is called the Euler-Bernoulli equation [1]. The distributed load $w(t, x)$ along the beam makes the equation non-homogeneous. Often in the following sections w will be taken equal to zero for simplification of the analysis.

2.1.3 Damping

Two different forms of damping are introduced to model the dissipation of energy during movement (structural damping) or during contact of the pipe with a surface.

Damping of vibrations

The damping of movements and vibrations of the beam, for example caused by friction with the seawater, can be modelled as a non-conservative external force F_d [N]. Although choosing a suitable model of friction and damping is highly depending on the application, a simple linear model is used in this research. The model is based on the *Rayleigh's dissipation function* [5] which makes the friction proportional to the velocity of the pipe, i.e. $F_d = -c_d \dot{y}$, and thus $F_d = -\frac{d}{dq} R$ with $R = 1/2(c_d \dot{q}^2)$. Because R does not depend on time explicitly, the Euler-Lagrange equations can be updated to include non-conservative external forces according to [5] to read

$$\frac{\partial \mathcal{L}}{\partial y} - \frac{\partial}{\partial t} \frac{\partial \mathcal{L}}{\partial \dot{y}} - \frac{\partial}{\partial x} \frac{\partial \mathcal{L}}{\partial y'} + \frac{\partial^2}{\partial t^2} \frac{\partial \mathcal{L}}{\partial \dot{y}} + \frac{\partial^2}{\partial t \partial x} \frac{\partial^2 \mathcal{L}}{\partial \dot{y} \partial y'} + \frac{\partial^2}{\partial x^2} \frac{\partial \mathcal{L}}{\partial y''} = -\frac{\partial R}{\partial \dot{q}}. \quad (2.10)$$

Using this form, the new partial differential equation including a damping coefficient reads

$$EIy'''' + c_d \dot{y} + \mu \ddot{y} = w, \quad (2.11)$$

again subject to the same initial and boundary conditions as (2.1).

The damping of movements during contact is discussed after the introduction of the modelling framework for contact, see Section 3.5.

2.1.4 Equilibrium

In the partial differential equations (2.9) and (2.11) the solution $y(t, x)$ depends on both time and location. It is interesting to analyze the *static problem*, which consists of excluding all time dependent terms from (2.6). This gives a new minimization problem given by

$$\min_y \int_0^L \frac{1}{2} EI (y'')^2 - w y dx, \quad (2.12)$$

which is minimized by the ordinary differential equation

$$EIy'''' = w \quad (2.13)$$

with some boundary conditions. Notice that (2.13) can also be found by excluding all time dependent terms in (2.9). In that case it is called the *equilibrium* of the partial differential equation.

In the following sections, often a distinction will be made between the (simpler) static problem and the dynamic problem. The static problem may be used to analyze certain properties of the behaviour of the solution such as shape, penetration of the contact surface or as an approximation to the dynamic problem with certain boundary conditions.

2.2 Three sections of beam

Using the Euler-Bernoulli equations, the pipe hanging in the sea can now be analyzed. To simplify this process, three sections of the pipe are identified (see fig. 2.1). First of all there is the section fixed to the ship which starts horizontally, rolls over the stinger with possibly permanent or alternating contact, and ends in a short piece of pipe which is guaranteed not to make contact with the stinger.

The second section is connected to the first section and is suspended above water. It will penetrate into the sea and the rest of the (mostly vertically) hanging section is submerged in the water. The bottom of the second section of the pipe must not make contact with the seabed.

The third and final section of the pipe is connected to the bottom of the second section and makes contact with the seabed. The end of the section is assumed to be fixed to the seabed, although in reality it will be held in place by an indefinite length of pipe laying still on the seabed.

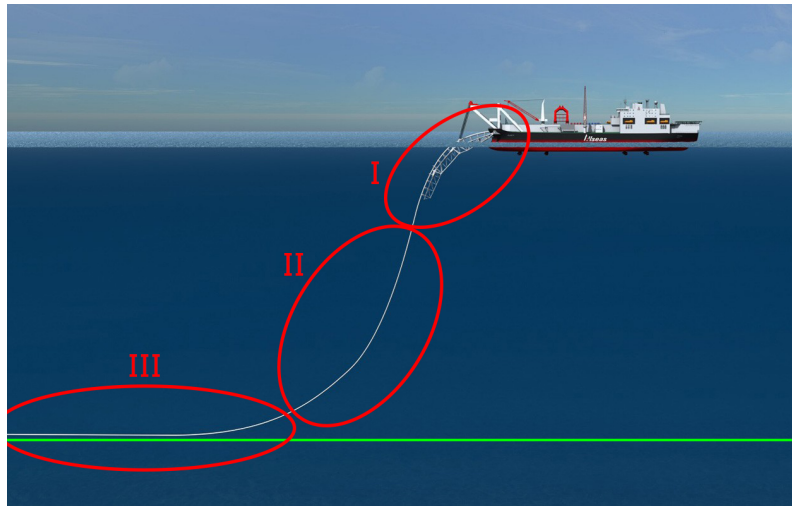


FIGURE 2.1: The S-lay method performed by an Allseas ship. The pipe is divided into three sections (indicated in red) which are analyzed separately. The contact surface (seabed) is indicated in green.

Chapter 3

Contact

For two of the sections of the pipe, contact must be enforced. There is a rich amount of literature available for modelling and solving contact problems. A starting point for this section has been [6] which describes the applicability of contact methods in the Finite Element Framework. These methods can be extended and solved with Lagrangian Multipliers [7, 8, 9].

This means that four things must be satisfied for a valid solution of the problem as given in (2.9), namely

1. the partial differential equation;
2. the boundary conditions;
3. the initial conditions;
4. no penetration of the surface where contact is enforced.

The enforcement of contact is defined in terms of penetration of a defined surface. This may be a constraint of the form $y(t, x) \geq 0$ for all t and x . Notice that such a requirement is not a requirement on the domain variables x and t , but rather a requirement on the entire solution. In particular even a simple translation of a solution can make the solution invalid. That is not usual for a linear partial differential equation. In practice when considering numerical solutions it is hard, if not impossible, to meet these requirements all together, let alone find such solutions efficiently.

In [10] a *power penalty* method is described for enforcing a constraint on the solution. The authors introduce a penalty in order to penalize penetration of contact surfaces. This research looks into multiple methods for enforcing contact, in order to find the best usable method for solving applicable problems. Three contact enforcement methods are considered, as described in [6], namely the *Penalty* method, the *Augmented Lagrangian* method and the *Augmented Barrier method*. All three methods introduce a penalty functional $\Xi(d_N(y))$ in the energy integral as given in (2.1) in order to create the integral minimization problem

$$\min_y \hat{J}(y) = \min_y \left(J(y) + \int_0^L \Xi(y) dx \right) = \min_y \int_0^L \frac{1}{2} EI (y'')^2 + \frac{1}{2} \mu (\dot{y})^2 + \Xi(d_N(y)) - w y dx, \quad (3.1)$$

which may be minimized to derive a partial differential equation. For each of the contact methods the form of Ξ is given, as well as the derivative with respect to d_N which will be required when the numerical integrations are derived in Section 4.1.7. The form of d_N is determined by the contact surface and subsequently the *gap*, discussed in Section 3.1. Note that the penalty does not always have a physical interpretation, depending on the form of Ξ . Also note that both Ξ and d_N may be non-linear functionals, which also makes the resulting minimization problem non-linear. Numerically, this means that equations will be solved using the Newton method.

3.1 Gap

The first requirement for modelling the contact is identifying the surface where contact is enforced. In this research the surface is a one dimensional function of the spatial variable x . We use an explicit function, although it

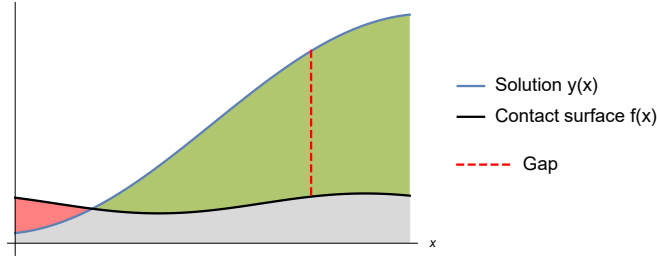


FIGURE 3.1: The gap between the solution and the contact surface. The green area indicates a positive gap (no contact violation), while the red area indicates a negative gap (contact violation).

is trivial to extend this assumption to an implicit function. It is also possible to extend this function to depend on the temporal variable t , which makes the surface change over time. For practical applications, the surface with contact will usually be higher dimensional in order to describe an object in two or three dimensional space.

In order to determine the penalty functional given in (3.1), the gap d_N [m] must be determined. This is the normal (minimal) distance between the surface and the object. In our one-dimensional problem with only up and down movements, this comes down to the vertical distance between the surface and the value of the deflection of the pipe (fig. 3.1). In higher-dimensional problems, the gap is a vector with a direction and a length.

To describe the shape of the contact surface, the function $f(x)$ is used. Then the solution y is constrained on $y \geq f(x)$ and the gap will become $d_N(y(x)) = y(x) - f(x)$ which is affine in y . Often in the following sections the contact surface will consist of the line $f(x) = 0$ with the restriction that the solution has to satisfy $y \geq 0$. This means that the normal distance between the solution and the contact surface equals $d_N = y$.

If the gap is positive ($d_N > 0$), there is no contact. Otherwise ($d_N \leq 0$), there is contact and the penalty functional will make sure that the contact is enforced as well as possible.

3.2 Penalty method

The Penalty method is the simplest method of the three considered methods. It is the only one which has a physical interpretation, and can be seen as a spring embedded in the surface where contact is enforced. The penalty functional Ξ is given by

$$\Xi(d_N) = \begin{cases} 0 & d_N > 0 \\ \frac{p}{2} d_N^2 & d_N \leq 0 \end{cases} \quad (3.2)$$

and its derivative with respect to d_N is given by

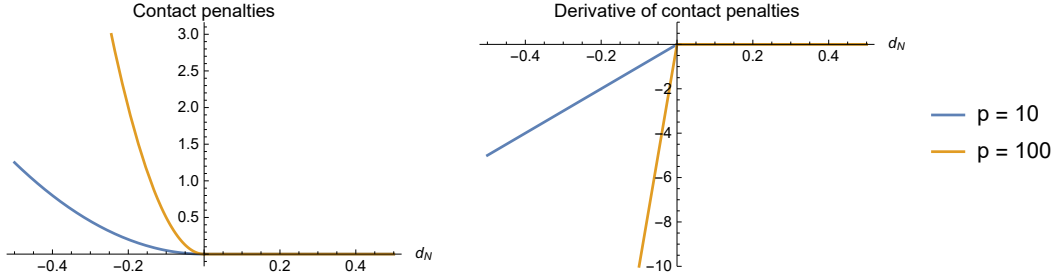
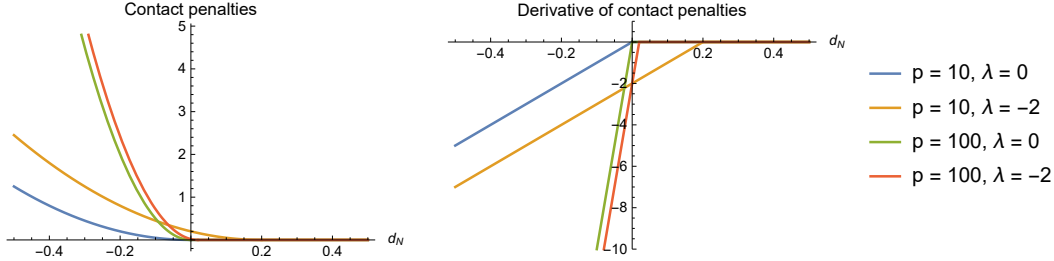
$$\nabla_{d_N} \Xi(d_N) = \begin{cases} 0 & d_N > 0 \\ p d_N & d_N \leq 0 \end{cases} \quad (3.3)$$

The parameter $p > 0$ is a penalty parameter. Notice that $\Xi(d_N)$ is a quadratic functional, which makes the resulting integral equation quadratic which may ease the solution process. However, also notice that the derivative of the penalty functional is not differentiable, exactly around the point of interest $d_N = 0$.

In figure fig. 3.2 the contact penalty $\Xi(d_N)$ is displayed with its derivative for multiple values of p .

3.3 Augmented Lagrangian method

In order to improve the performance of the Penalty method, a Lagrangian method can be used. In addition to p , it has a parameter $\lambda(x) \leq 0$ which acts as a way to ‘remember’ contact, provide stability to numerical methods and reduce the effect of non-linearities in the equations.


 FIGURE 3.2: contact penalties $\Xi(d_N)$ and the their derivatives for the Penalty method with $d_N \in [-0.5, 0.5]$.

 FIGURE 3.3: The contact penalties $\Xi(d_N)$ and the their derivatives for the Augmented Lagrangian method with $d_N \in [-0.5, 0.5]$.

For the Augmented Lagrangian method the penalty functional is augmented and becomes to

$$\Xi(d_N) = \begin{cases} 0 & \lambda + pd_N > 0 \\ \frac{1}{2p}(\lambda + pd_N)^2 & \lambda + pd_N \leq 0 \end{cases} \quad (3.4)$$

and its derivative with respect to d_N is given by

$$\nabla_{d_N} \Xi(d_N) = \begin{cases} 0 & \lambda + pd_N > 0 \\ \lambda + pd_N & \lambda + pd_N \leq 0 \end{cases}. \quad (3.5)$$

The contact penalty and its derivative are displayed in fig. 3.3 for some values of p and λ . See [6], section 3.4.2, for an in-depth explanation of the reason for choosing λ in this way.

3.4 (Augmented) Barrier method

The Augmented Barrier method is introduced as a way to not only provide numerical stability, but also to increase the penalty levels in case of large penetrations. Instead of using a quadratic functional, a logarithmic functional is used. First a naive method is considered (Barrier method) which is then expanded and augmented to deduce the Augmented Barrier method.

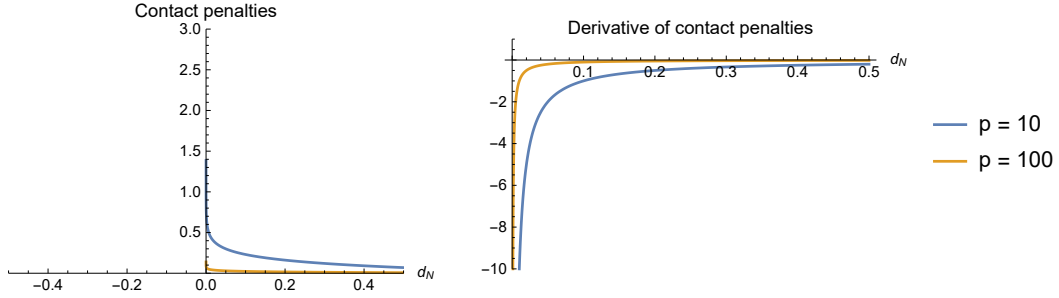
3.4.1 Barrier method

A logarithmic form is introduced by setting the penalty functional to

$$\Xi(d_N) = -\frac{1}{p} \log(d_N) \quad (3.6)$$

which has a derivative with respect to d_N of the form

$$\nabla_{d_N} \Xi(d_N) = -\frac{1}{pd_N}. \quad (3.7)$$


 FIGURE 3.4: The contact penalties $\Xi(d_N)$ and the their derivatives for the Barrier method with $d_N \in [-0.5, 0.5]$.

This functional has the property that it is undefined for values of $d_N \leq 0$. For theoretical applications the method should work well. Around the value of $d_N = 0$ a barrier is erected which becomes steeper as the value of p increases, tending to a penalty of ∞ for $d_N = 0$. This behaviour should model the requirement that $d_N \geq 0$ perfectly: the solution never violates the contact surface. In figure 3.4 a visualization of the Barrier and the derivative with respect to d_N is shown.

However, notice that even for $d_N > 1$ (a valid solution), the penalty term $\Xi(d_N)$ is non-zero and even negative. This means that the solution is pushed away from the barrier if it is close to the barrier $d_N = 0$, but it is pushed *towards* the barrier if it is far away from it. This effect is reduced for large values of p .

There are two problems with this method. Because of the penalty functional tending to very large values around the asymptote, the conditioning of the numerical problem becomes worse as the value of p is increased. In addition to that, during the process of solving the minimization problem it may occur that before convergence of the solution it violates the requirement $d_N \geq 0$ for a short time. However, the penalty does not exist there and the penalty functional is undefined for those values. By extending the penalty functional it will never be undefined during the numeric solution process.

For this reason the Barrier method is both augmented and extended in order to form the Augmented Barrier method.

3.4.2 Augmented Barrier method

The Barrier is shifted such that the asymptote moves towards negative values of d_N , and a Lagrangian parameter $\lambda(x)$ is added. Finally, the barrier functional has been extended with a quadratic functional such that the penalty functional is defined for all values of d_N . The new functional is given by

$$\Xi(d_N) = \begin{cases} \frac{\lambda}{p} \log(s + p d_N) & d_N \geq -\frac{\beta s}{p} \\ \frac{\lambda}{p} \left(-\frac{p^2}{2(s(1-\beta))^2} d_N^2 + \frac{(p(1-2\beta))}{s(1-\beta)^2} d_N + \frac{\beta(2-3\beta)}{2(1-\beta)^2} + \log(s(1-\beta)) \right) & d_N < -\frac{\beta s}{p} \end{cases} \quad (3.8)$$

with derivative

$$\nabla_{d_N} \Xi(d_N) = \begin{cases} \lambda \frac{1}{p d_N + s} & d_N \geq -\frac{\beta s}{p} \\ \lambda \frac{-p d_N - 2\beta s + s}{(\beta - 1)^2 s^2} & d_N < -\frac{\beta s}{p} \end{cases} \quad (3.9)$$

The contact penalty and its derivative are displayed in fig. 3.5 for some values of p and λ .

Notice that several parameters have been added. The parameter $p > 0$ is still a penalty parameter and controls how well the contact must be enforced. Furthermore, $s \in [1, s_{\max}]$ is a scaling parameter which may be used to scale the penalty if more than one barrier is used when solving a contact problem. The value of s_{\max} may be set to a large value such that the scaling does not reduce the effectiveness of the method (see [6] for more information). Finally the parameter $\beta \in (0, 1)$ controls how far between $d_N = 0$ and $d_N = -s/p$ (the logarithmic asymptote) the functional changes to the quadratic form. The coefficients of the quadratic continuation are chosen (uniquely) such that the entire functional Ξ is continuous and differentiable in d_N .¹

¹In [6] there is an error in the formula for Ξ (page 44, top). In the case for $d_N < (-\beta s)/p$, the Lagrangian and penalty parameters are missing making the functional discontinuous. In (3.8) and (3.9) these terms have been added.

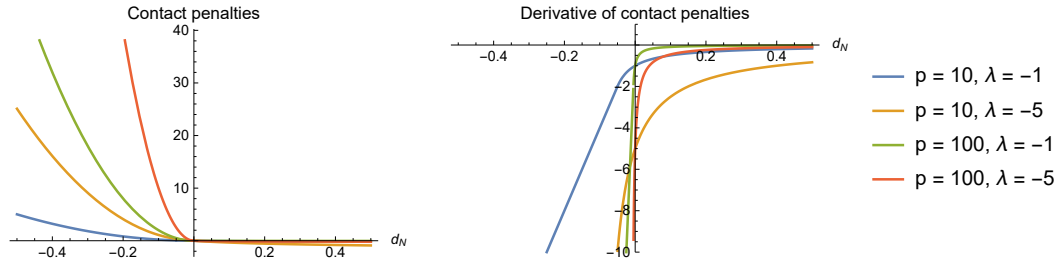


FIGURE 3.5: The contact penalties $\Xi(d_N)$ and the their derivatives for the Augmented Barrier method with $d_N \in [-0.5, 0.5]$.

3.5 Damping on contact

In addition to structural damping, there are also possibilities to model damping during contact. This allows adding certain properties of materials. A common application is the seabed, where the surface is made of sand, mud or some other soft material. In this case, energy will be lost on contact and some kinetic energy will be absorbed by the surface. Note that there are other contact situations where bounces because of contact and preservation of kinetic energy are realistic. This may be the case when the pipe makes contact with a metal surface like on the stinger of the ship. In those cases no damping on contact should be added to the model.

The contact is modelled in a similar way as the structural damping of the entire beam. It is seen as a resistance force in the opposite direction to the contact velocity \dot{d}_N . The magnitude of the resistance force depends on a damping parameter c_c . The damping is active only close to the surface, or whenever the solution has penetrated the surface (the gap d_N is negative), which is characterized by the parameter ε_g . This gives a combined model for a 'drag force' F_c [N], given by

$$F_c(\dot{d}_N) = \begin{cases} 0 & d_N > \varepsilon_g \\ -c_c \dot{d}_N & d_N \leq \varepsilon_g \end{cases}. \quad (3.10)$$

The parameter ε_g is added to make sure that damping occurs even when the contact methods perform well, i.e. the number of time steps spent below the contact surface (in violation of the contact requirement) is small. To increase the places where the solution is damped, the region of contact is expanded to allow more drag, even when no contact occurs. In particular this is needed when a contact method with a high valued penalty parameter is used. In that case, there is almost no contact violation, which would result in almost no damping caused by contact. By making the value of ε_g non-zero, a small region above the contact surface also causes the solution to be damped.

Notice that in the expression for F_c the argument \dot{d}_N is used instead of \dot{y} . For a one-dimensional problem this makes no difference, but for higher-dimensional problems the direction of the drag depends on the shape of the surface and the direction of movement in comparison to the surface.

3.6 Updating rules

This chapter describes contact methods which have a penalty parameter p and may have a Lagrangian parameter $\lambda(x)$. These parameters do not have to have a fixed value but are rather updated between steps in the solution process of a static or dynamic problem. For the dynamic problem time integration steps are taken, and each time step the Newton method is used to solve the equations because of the non-linearity of the equations (see Chapter 4). For the static problem only Newton steps are required to find a solution. The value of $\lambda(x)$ is then updated and this is repeated until a good solution is found. the following sections are a discussion on when and how the values of p and λ are updated.

3.6.1 Updating rule of p

In all of the contact enforcement methods, a penalty parameter p is present. This parameter determines how well the contact (or the constraint on the solution) is enforced. For each of the methods, this parameter may vary

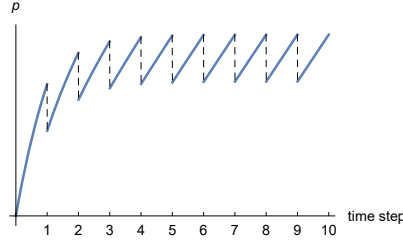


FIGURE 3.6: The increasing of the value of p during each time step, while letting the value converge over time to a stationary p .

in value and in particular may change during solution iterations. A distinction is made between the static and dynamic problem.

Static problem For the static problem (no time component, equilibrium) given in (2.13), it is advisable to increase the value of p during multiple iterations of the solution process [6]. The value will be initialized at some value $p_0 > 0$, and be increased each iteration (usually a Newton iteration, but possibly something else) with a factor $\psi \geq 1$. After n iterations, the value of p will be $p_0\psi^{n-1}$. By increasing the value of p during the solution process, the solution of the previous value of p is known and used to find a new solution improved contact enforcement.

A higher value of p will enforce the contact better, but the numerical stability may decrease, due to larger differences in the order of values in the calculations. For example, for too large values of p the penalty functional will dominate the contact requirement over the problem structure. For this reason it is a good idea to analyze a maximum value of p per application to make sure no large numerical errors occur in any stage of the solving process.

Dynamic problem For solving the dynamic problem, the situation is different. Assuming that the initial condition y_0 does not violate any surface where contact is enforced, a high value of p can be used to calculate the solution at the next time step, for a single time iteration step (Section 4.1.7). After all, a previous solution is known which is ‘close’ to the new solution, assuming the time step is small enough.

In addition, it does not make sense to increase the value of p during a time iteration step (see fig. 3.6). The previous solution is known, and by decreasing the value of p a lot in order to increase it again slowly during the time-step solution iterations will destroy the knowledge in the previous solution. Any enforced contact at the previous time step will be reduced with a lower p and slowly restored during the increase of p during the time integration step.

It is clear that this is not an efficient way to do a time integration step, so a constant value of p is used ($\psi = 1$) for dynamic problems.

3.6.2 Updating rules of λ

In the Augmented Lagrangian and Augmented Barrier methods, a Lagrangian parameter $\lambda(x)$ is present. This parameter is updated discretely using the penalty functional Ξ and the *next* value of p . The value of λ is initialized with some function $\lambda_0(x)$, usually a constant. The initial value does not influence the working of the contact methods, except for the first few time steps. The allowed values of λ_0 depend on the contact method.

In order to update the value of λ , two things are required. The update rule gives the new value, and the update scheme provides the times or steps when the update rule is applied.

We can use the penalty functional and update λ^- to the new value λ^+ using

$$\lambda^+ = \nabla_{d_N} \Xi(d_N; \lambda^-). \quad (3.11)$$

This expression can be deduced from the Lagrangian minimization condition [6]. Additionally, a variation of the update rule for λ has been designed for numerical stability. Instead of updating the entire value of λ , a linear combination of the old and the updated value is used, determined by a parameter $\eta \in [0, 1]$, given by

$$\lambda^+ = \eta\lambda^- + (1 - \eta)\nabla_{d_N} \Xi(d_N; \lambda^-). \quad (3.12)$$

The extreme value $\eta = 0$ gives the original update rule (3.11) and $\eta = 1$ gives a constant function $\lambda = \lambda_0$ for each update step.

Determining the scheme when to update the value of λ for the static problem is straightforward. Each iteration of the method, the value of λ is updated once before finding the Newton method solution for that iteration. For the dynamic problem, two schemes for updating λ have been made. *Scheme 1* updates the value of λ each Newton iteration (multiple times per time step), while *Scheme 2* updates the value of λ only after each time step. Using *Scheme 1*, the value of λ is updated more often, but non-final solutions within the Newton method are used which may not be helpful for the contact method. *Scheme 2* however uses old ‘information’ of the previous time step, which may harm the performance and stability for the Newton convergence. Both schemes are compared in Section 6.2.2.

Chapter 4

Analysis: Finite Element Method

In this chapter the Finite Element expressions for the model of the pipe are derived. Using those expressions, a numerical integration scheme is given which is used to integrate the dynamic problem. Finally, a *reference solution* will be constructed which is used to benchmark the convergence of the numerical methods.

4.1 Finite element derivation

The Finite Element Method [11, 12] has been used for solving the minimization problem (2.6) numerically. More specifically, [13] discusses Finite Element considerations and common assumptions for solving problems involving beams and frames. As discussed in Section 2.1, only small deflections are allowed. This allows a simpler linear Finite Element model, but restricts the solutions to only small parts of the pipe. In order to find a representation of the entire beam, a non-linear Finite Element model must be taken such as the *co-rotational method*. That method is discussed extensively in [14] and for examples the reader is referred to [15]. For simplicity of the derivations, the linear Finite Element model is used here which suits the purposes of this research. However, note that the following derivations can be repeated even if other Finite Element method assumptions are made.

The spatial domain $[0, L]$ is divided into a partition of N ordered elements, not necessarily of equal length. The partition will have $N + 1$ points (nodes) x_k with $x_0 = 0$ and $x_N = L$ and $x_{k+1} > x_k$ for $k \in \{0, \dots, N-1\}$. The subdomains between consecutive points are *elements*, denoted by e_k with $k \in \{1, \dots, N\}$ (the first element e_1 connects x_0 and x_1). The length of element e_k is given by $L_k = x_k - x_{k-1}$. As all of the following derivations are only in the spatial direction, the solution $y(t, x)$ is denoted with $y_t(x)$.

For each node x_k we now have two degrees of freedom: the value of $y_{t,k} = y_t(x_k)$ and the value of $\vartheta_{t,k} = y'_t(x_k)$. This means each element e_k has four degrees of freedom: two for each connecting node. For each element we define four basis functions on that element, given by

$$\begin{aligned}\phi_1(\xi_k) &= 1 - 3\xi_k^2 + 2\xi_k^3 & \phi_2(\xi_k) &= L_k \left(\xi_k - 2\xi_k^2 + \xi_k^3 \right) \\ \phi_3(\xi_k) &= 3\xi_k^2 - 2\xi_k^3 & \phi_4(\xi_k) &= L_k \left(-\xi_k^2 + \xi_k^3 \right)\end{aligned}\tag{4.1}$$

where ξ_k is an element-local coordinate given by $\xi_k = (x - x_{k-1})/L_k$ and L_k is the length of the element. Outside the domain of the element, the basis functions equal 0. The basis functions are *Hermite Cubic Shape Functions* on $[0, 1]$. The functions are derived in Appendix A.1. See fig. 4.1 for a visualization of a single element.

The solution y of the minimization problem (2.6) is now represented by

$$y(t, x) = y_t(x) = \sum_{k=1}^N y_{t,k-1} \phi_1(\xi_k) + \vartheta_{t,k-1} \phi_2(\xi_k) + y_{t,k} \phi_3(\xi_k) + \vartheta_{t,k} \phi_4(\xi_k).\tag{4.2}$$

This is a function of $x \in [0, L]$ since the ξ_k are an affine linear function of x . The function has $2(N + 1)$ parameters, namely $y_{t,k}$ and $\vartheta_{t,k}$ for $k \in \{0, \dots, N\}$. Notice that $y_t(x)$ is continuous and differentiable in the spatial direction x . Note that for some node x_k , the shape functions of two elements connect in a continuously differentiable way,

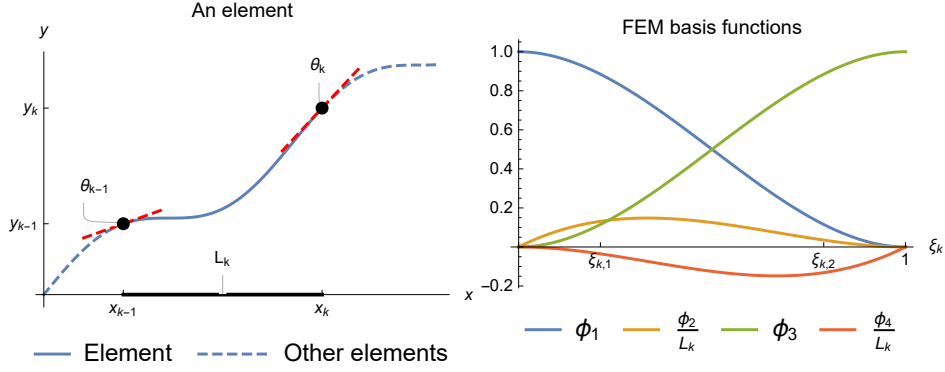


FIGURE 4.1: Left: an element with its coordinates, derivative and length. Right the Finite Element basis functions with the Gauss associated integration points $\xi_{k,1}$ and $\xi_{k,2}$ for k the element index.

such that the value of y_k and θ_k are equal to $y_t(x_k)$ and $y'_t(x_k)$. We can also write (4.2) as

$$y_t(x) = \sum_k N(\xi_k) q_{t,k} \quad (4.3)$$

with

$$N(\xi_k) = (\phi_1(\xi_k), \phi_2(\xi_k), \phi_3(\xi_k), \phi_4(\xi_k)), \quad q_{t,k} = (y_{t,k-1}, \vartheta_{t,k-1}, y_{t,k}, \vartheta_{t,k})^\top. \quad (4.4)$$

Furthermore the $q_{t,k}$ can also be written as $q_{t,k} = P_k q_t$ if we define

$$q_t = (y_{t,0}, \vartheta_{t,0}, y_{t,1}, \vartheta_{t,1}, \dots, y_{t,N}, \vartheta_{t,N})^\top. \quad (4.5)$$

The P_k are permutation matrices of dimension $4 \times 2(N+1)$ (for N elements) that position the element coefficients $q_{t,k}$ into the larger q_t vector. They are of the form

$$P_k = \begin{pmatrix} O_{4 \times (2k-2)} & I_{4 \times 4} & O_{4 \times (2N-2k)} \end{pmatrix}. \quad (4.6)$$

4.1.1 Stiffness matrix

In order to determine the stiffness matrix K , the first term of (2.6) given by

$$\int_0^L EI (y''_t)^2 dx \quad (4.7)$$

is integrated. Using the substitution (4.2) we find

$$\begin{aligned} \int_0^L EI (y''_t)^2 dx &= \int_0^L \sum_k EI \frac{1}{L_k^4} q_{t,k}^\top N''(\xi_k)^\top N''(\xi_k) q_{t,k} dx \\ &= q_t^\top \left(\sum_k P_k^\top \frac{EI}{L_k^3} \int_0^1 N''(\xi_k)^\top N''(\xi_k) d\xi_k P_k \right) q_t \\ &= q_t^\top \left(\sum_k P_k^\top K_k P_k \right) q_t \\ &= q_t^\top K q_t. \end{aligned} \quad (4.8)$$

In (4.8) we use that

$$N''(\xi_k) = \begin{pmatrix} 12\xi_k - 6 & L(6\xi_k - 4) & 6 - 12\xi_k & L(6\xi_k - 2) \end{pmatrix}, \quad (4.9)$$

such that we can conclude

$$\begin{aligned}
 K_k &= \frac{EI}{L_k^3} \int_0^1 N''(\xi)^\top N''(\xi) d\xi \\
 &= \frac{EI}{L_k^3} \int_0^1 \begin{pmatrix} (6-12\xi)^2 & (6\xi-4)(12\xi-6)L_k & -36(1-2\xi)^2 & (6\xi-2)(12\xi-6)L_k \\ (6\xi-4)(12\xi-6)L_k & (4-6\xi)^2 L_k^2 & (6-12\xi)(6\xi-4)L_k & (6\xi-4)(6\xi-2)L_k^2 \\ -36(1-2\xi)^2 & (6-12\xi)(6\xi-4)L_k & (6-12\xi)^2 & (6-12\xi)(6\xi-2)L_k \\ (6\xi-2)(12\xi-6)L_k & (6\xi-4)(6\xi-2)L_k^2 & (6-12\xi)(6\xi-2)L_k & (2-6\xi)^2 L_k^2 \end{pmatrix} d\xi \\
 &= \frac{EI}{L_k^3} \begin{pmatrix} 12 & 6L_k & -12 & 6L_k \\ 6L_k & 4L_k^2 & -6L_k & 2L_k^2 \\ -12 & -6L_k & 12 & -6L_k \\ 6L_k & 2L_k^2 & -6L_k & 4L_k^2 \end{pmatrix}, \tag{4.10}
 \end{aligned}$$

and $K = \sum_k P_k^\top K_k P_k$. Notice the subscript k has been stripped of the ξ_k argument in the integration for more clearness.

4.1.2 Mass matrix

Similarly to the K matrix, we can also deduce the form of the mass matrix M . In some literature the density ρ and the cross-section area per unit length A may be found instead of the mass per unit length of the beam μ . The relation $\mu = \rho A$ holds. This matrix is not used in calculations for the static problem (2.13).

The mass matrix is determined from the term

$$\int_0^L \mu (\dot{y}_t)^2 dx \tag{4.11}$$

in (2.6). We substitute (4.2) in the form $y_t(x) = \sum_k N(\xi_k) q_{t,k}$ into (4.11) and find

$$\begin{aligned}
 \int_0^L \mu \dot{y}_t^2 dx &= \int_0^L \sum_k \mu \dot{q}_{t,k}^\top N(\xi_k)^\top N(\xi_k) \dot{q}_{t,k} dx \\
 &= \dot{q}_t^\top \left(\sum_k P_k^\top \mu L_k \int_0^1 N(\xi_k)^\top N(\xi_k) d\xi_k P_k \right) \dot{q}_t \\
 &= \dot{q}_t^\top \left(\sum_k P_k^\top M_k P_k \right) \dot{q}_t \\
 &= \dot{q}_t^\top M \dot{q}_t, \tag{4.12}
 \end{aligned}$$

where the M_k are determined by evaluating

$$\begin{aligned}
 M_k &= \mu L_k \int_0^1 N(\xi)^\top N(\xi) d\xi \\
 &= \mu L_k \int_0^1 \begin{pmatrix} (\xi-1)^4 (2\xi+1)^2 & (\xi-1)^4 \xi (2\xi+1) L_k & (3-2\xi)(\xi-1)^2 \xi^2 (2\xi+1) & (\xi-1)^3 \xi^2 (2\xi+1) L_k \\ (\xi-1)^4 \xi (2\xi+1) L_k & (\xi-1)^4 \xi^2 L_k^2 & (3-2\xi)(\xi-1)^2 \xi^3 L_k & (\xi-1)^3 \xi^3 L_k^2 \\ (3-2\xi)(\xi-1)^2 \xi^2 (2\xi+1) & (3-2\xi)(\xi-1)^2 \xi^3 L_k & (3-2\xi)^2 \xi^4 & (3-2\xi)(\xi-1) \xi^4 L_k \\ (\xi-1)^3 \xi^2 (2\xi+1) L_k & (\xi-1)^3 \xi^3 L_k^2 & (3-2\xi)(\xi-1) \xi^4 L_k & (\xi-1)^2 \xi^4 L_k^2 \end{pmatrix} d\xi \\
 &= \frac{\mu L_k}{420} \begin{pmatrix} 156 & 22L_k & 54 & -13L_k \\ 22L_k & 4L_k^2 & 13L_k & -3L_k^2 \\ 54 & 13L_k & 156 & -22L_k \\ -13L_k & -3L_k^2 & -22L_k & 4L_k^2 \end{pmatrix}. \tag{4.13}
 \end{aligned}$$

Notice the subscript k has been stripped of the ξ_k argument in the integration for more clearness.

4.1.3 Damping matrix

The damping matrix can be seen as the factor by which the velocity \dot{q} is multiplied in order to define a dissipative damping force. This matrix is not used in calculations for the static problem (2.13).

Using the Finite Element method, the damping matrix cannot be simply derived in the same way as the mass and stiffness matrices, because the damping is modelled as an external dissipation of energy which does not exist in the minimization problem. However, a common way to add damping in the Finite Element system of equations is by adding a damping matrix $C = \alpha_1 M + \alpha_2 K$ (as proposed in [16]) which is called *proportional damping* (or *Rayleigh damping*) and assumes uniform energy dissipation. The actual values of α_1 and α_2 depend on the structural damping properties.

4.1.4 Finite element derivation for contact

Gauss-Legendre interpolation

A common method to evaluate the penalty term $\Xi(d_N)$ in (3.1) is by using a simple trapezoidal integration rule. This section explains the use of Gauss-Legendre interpolation to achieve a higher accuracy for evaluating the contact penalty integral while using the Finite Element method.

We minimize the energy functional with the added contact penalty terms given by the problem

$$\min_y \int_0^L \frac{1}{2} EI (y'')^2 + \frac{1}{2} \mu \dot{y}^2 + \Xi_1(d_N) + \Xi_2(\dot{d}_N) dx \quad (4.14)$$

which describes the beam with enforced contact. The functional Ξ_i , $i \in \{1, 2\}$ is some (possibly non-linear) penalty function which penalizes contact violation or introduces damping. The derivation below is made for a general function Ξ , which can be substituted by Ξ_1 or Ξ_2 . Even then, the methods below can be expanded for functions of more variables, although the calculations become less clear.

In the derivation below we make explicit use of the affine form of d_N in terms of y . For higher-dimensional problems the normal distance will be defined in a non-linear fashion, which may cause some of the derivatives to consist a few more terms.

The basic trapezoidal rule for evaluating the integral of a given function $g(x)$ on the interval $[a, b]$ is given by the approximation

$$\int_a^b g(x) dx \approx \frac{g(b) + g(a)}{2} (b - a), \quad (4.15)$$

which is the length of the interval times the average function value on the interval. One of the widely used methods is Gauss-Legendre interpolation [17]. This method improves the numerical precision by choosing the points of discretization x_j and weights ζ_j with $j \in \{1, 2\}$. They are chosen such that the approximation

$$\int_{-1}^1 g(x) dx \approx \sum_{j=1}^m \zeta_j g(x_j) \quad (4.16)$$

is exact for polynomials of order $2m - 1$. For $m = 2$ we use four linear independent polynomials of maximal degree three, for example $1, x, x^2, x^3$, and determine the values for x_j and ζ_j by solving the four equations

$$\begin{aligned} \int_{-1}^1 1 dx &= 2 = \zeta_1 + \zeta_2 & \int_{-1}^1 x dx &= 0 = \zeta_1 x_1 + \zeta_2 x_2 \\ \int_{-1}^1 x^2 dx &= \frac{2}{3} = \zeta_1 x_1^2 + \zeta_2 x_2^2 & \int_{-1}^1 x^3 dx &= 0 = \zeta_1 x_1^3 + \zeta_2 x_2^3. \end{aligned} \quad (4.17)$$

This results in $\zeta_1 = \zeta_2 = 1$ and the points x_j given by $x_{1,2} = \pm \sqrt{1/3}$. Thus the integral of g is approximated as

$$\int_{-1}^1 g(x) dx \approx \zeta_1 g(x_1) + \zeta_2 g(x_2) = g(-\sqrt{1/3}) + g(\sqrt{1/3}). \quad (4.18)$$

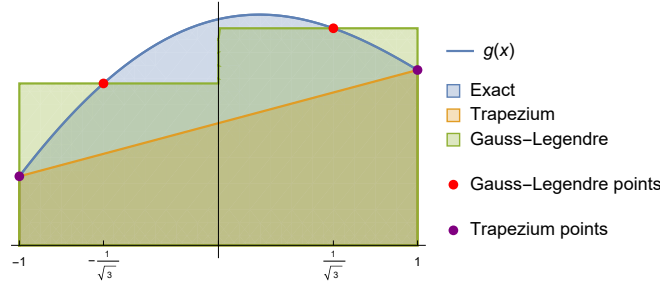


FIGURE 4.2: A comparison of the integration points and area between the trapezium and Gauss-Legendre integration approximations for the integral of some function $g(x)$ over the interval $[-1, 1]$.

This method of numerical integration by finding points and weights in an interval can be extended to any number of points. For an approximation of m points, the evaluation points of g will interestingly turn out to be the zeros of Legendre polynomials P_m . This means that the points x_j can be found without the use of the equations in (4.17). The weights ζ_j will still have to be solved using the integral equations in (4.17). The approximation of the integral will be exact for polynomials of order up to $2m - 1$. In fig. 4.2 a visual comparison between the integration methods is given.

Finite Element integration

The Gauss-Legendre integral approximation is now applied to the Finite Element framework. The assumption made in (4.2) is applied to the solution y . The subscript t is dropped from the following calculations for clarity. Also the affine one-dimensional structure of $d_N(y) = y - f(x)$ is used explicitly. Then Ξ -integral is approximated as

$$\begin{aligned} \int_0^L \Xi(y(x) - f(x)) dx &= \sum_k L_k \int_0^1 \Xi(y_{k-1}\phi_1(\xi_k) + \vartheta_{k-1}\phi_2(\xi_k) + y_k\phi_3(\xi_k) + \vartheta_k\phi_4(\xi_k) - f(\xi_k)) d\xi_k \\ &\approx \sum_k L_k \sum_{j=1}^2 \zeta_j \Xi(y_{k-1}\phi_1(\xi_{k,j}) + \vartheta_{k-1}\phi_2(\xi_{k,j}) + y_k\phi_3(\xi_{k,j}) + \vartheta_k\phi_4(\xi_{k,j}) - f(\xi_{k,j})) \\ &= \sum_{j=1}^2 \zeta_j \sum_k L_k \Xi(y_{k-1}\phi_1(\xi_{k,j}) + \vartheta_{k-1}\phi_2(\xi_{k,j}) + y_k\phi_3(\xi_{k,j}) + \vartheta_k\phi_4(\xi_{k,j}) - f(\xi_{k,j})). \end{aligned} \quad (4.19)$$

Notice that $\zeta_1 = \zeta_2 = 1/2$ and $\xi_{k,1} = (1 - \sqrt{1/3})/2$, $\xi_{k,2} = (1 + \sqrt{1/3})/2$ must be used, which is caused by the transformation of Gauss-Legendre interpolation from the interval $[x_{k-1}, x_k]$ of element k to the $[0, 1]$ interval. Also notice that the $\xi_{k,j}$ are the same numerical value for each element, but correspond to different values of x (this is important when evaluating $f(\xi_{k,j})$).

We differentiate (4.19) two times with respect to $q = (y_0, \vartheta_0, y_1, \vartheta_1, \dots, y_N, \vartheta_N)^T$ (using N elements), which is used in the Finite Element formulation calculated later. Deriving the integral to q yields

$$\begin{aligned} \frac{d}{dq} \left(\int_0^L \Xi(y(x) - f(x)) dx \right) &\approx \sum_{j=1}^2 \zeta_j \begin{pmatrix} \phi_1(\xi_{1,j}) & 0 & 0 & \dots \\ \phi_2(\xi_{1,j}) & 0 & 0 & \dots \\ \phi_3(\xi_{1,j}) & \phi_1(\xi_{2,j}) & 0 & \dots \\ \phi_4(\xi_{1,j}) & \phi_2(\xi_{2,j}) & 0 & \dots \\ 0 & \phi_3(\xi_{2,j}) & \phi_1(\xi_{3,j}) & \dots \\ 0 & \phi_4(\xi_{2,j}) & \phi_2(\xi_{3,j}) & \dots \\ \vdots & \vdots & \vdots & \ddots \end{pmatrix} \begin{pmatrix} L_1 \Xi'(y_0\phi_1(\xi_{1,j}) + \vartheta_0\phi_2(\xi_{1,j}) + y_1\phi_3(\xi_{1,j}) + \vartheta_1\phi_4(\xi_{1,j}) - f(\xi_{1,j})) \\ L_2 \Xi'(y_1\phi_1(\xi_{2,j}) + \vartheta_1\phi_2(\xi_{2,j}) + y_2\phi_3(\xi_{2,j}) + \vartheta_2\phi_4(\xi_{2,j}) - f(\xi_{2,j})) \\ L_3 \Xi'(y_2\phi_1(\xi_{3,j}) + \vartheta_2\phi_2(\xi_{3,j}) + y_3\phi_3(\xi_{3,j}) + \vartheta_3\phi_4(\xi_{3,j}) - f(\xi_{3,j})) \\ \vdots \end{pmatrix} \\ &= \sum_{j=1}^2 \zeta_j A_j V_j(q). \end{aligned} \quad (4.20)$$

Consider the matrix and vector sizes. The matrix A_j is a $(2N+2) \times N$ matrix, and the vector $V_j(q)$ has length N . Together this gives a vector of length $2N+2$. The second derivative to q of (4.19) can then be found to be

$$\begin{aligned}
 \frac{d^2}{dq^2} \left(\int_0^L \Xi(y(x) - f(x)) dx \right) &\approx \frac{d}{dq} \left(\sum_{j=1}^2 \varsigma_j A_j V_j(q) \right) \\
 &= \sum_{j=1}^2 \varsigma_j A_j \text{diag} \begin{pmatrix} L_1 \Xi''(y_0 \phi_1(\xi_{1,j}) + \vartheta_0 \phi_2(\xi_{1,j}) + y_1 \phi_3(\xi_{1,j}) + \vartheta_1 \phi_4(\xi_{1,j}) - f(\xi_{1,j})) \\ L_2 \Xi''(y_1 \phi_1(\xi_{2,j}) + \vartheta_1 \phi_2(\xi_{2,j}) + y_2 \phi_3(\xi_{2,j}) + \vartheta_2 \phi_4(\xi_{2,j}) - f(\xi_{2,j})) \\ L_3 \Xi''(y_2 \phi_1(\xi_{3,j}) + \vartheta_2 \phi_2(\xi_{3,j}) + y_3 \phi_3(\xi_{3,j}) + \vartheta_3 \phi_4(\xi_{3,j}) - f(\xi_{3,j})) \\ \vdots \end{pmatrix} \\
 &\quad \begin{pmatrix} \phi_1(\xi_{1,j}) & \phi_2(\xi_{1,j}) & \phi_3(\xi_{1,j}) & \phi_4(\xi_{1,j}) & 0 & 0 & & \\ 0 & 0 & \phi_1(\xi_{2,j}) & \phi_2(\xi_{2,j}) & \phi_3(\xi_{2,j}) & \phi_4(\xi_{2,j}) & \dots & \\ 0 & 0 & 0 & 0 & \phi_1(\xi_{3,j}) & \phi_2(\xi_{3,j}) & & \\ & & \vdots & & & & & \ddots \end{pmatrix} \\
 &= \sum_{j=1}^2 \varsigma_j A_j J_j(q) A_j^T, \tag{4.21}
 \end{aligned}$$

where the $J_j(q)$ have size $N \times N$, which makes the Jacobian a $(2N+2) \times (2N+2)$ matrix, as it should be.

The values of the basis functions ϕ_i , $i \in \{1, \dots, 4\}$ at the interpolation points $\xi_{k,1} = (1 - \sqrt{1/3})/2$ and $\xi_{k,2} = (1 + \sqrt{1/3})/2$ are given by

$$\begin{aligned}
 \phi_1(\xi_{k,1}) &= \frac{1}{18} (9 + 4\sqrt{3}) \approx 0.8849 & \phi_2(\xi_{k,1}) &= \frac{L_k}{36} (3 + \sqrt{3}) \approx 0.1314L_k \\
 \phi_3(\xi_{k,1}) &= \frac{1}{18} (9 - 4\sqrt{3}) \approx 0.1151 & \phi_4(\xi_{k,1}) &= \frac{L_k}{36} (-3\sqrt{3}) \approx 0.0352L_k \\
 \phi_1(\xi_{k,2}) &= \frac{1}{18} (9 - 4\sqrt{3}) \approx 0.1151 & \phi_2(\xi_{k,2}) &= -\frac{L_k}{36} (-3\sqrt{3}) \approx 0.0352L_k \\
 \phi_3(\xi_{k,2}) &= \frac{1}{18} (9 + 4\sqrt{3}) \approx 0.8849 & \phi_4(\xi_{k,2}) &= -\frac{L_k}{36} (3 + \sqrt{3}) \approx -0.1314L_k. \tag{4.22}
 \end{aligned}$$

The symmetry is obvious.

4.1.5 Distributed load

The distributed load $w_t(x)$ can be approximated by a load vector F_t . The term

$$\int_0^L w_t y dx \tag{4.23}$$

in (2.6) is integrated. The substitution in (4.2) of the form $y_t(x) = \sum_k N(\xi_k) q_{t,k}$ is used for (4.23). We find

$$\begin{aligned}
 \int_0^L w_t y dx &= \int_0^L w_t(\xi_k) \sum_k N(\xi_k) q_{t,k} dx \\
 &= \left(\sum_k L_k \int_0^1 w_t(\xi_k) N(\xi_k) d\xi_k P_k \right) q_t \\
 &= \left(\sum_k F_{t,k}^T P_k \right) q_t \\
 &= F_t^T q_t, \tag{4.24}
 \end{aligned}$$

where the $F_{t,k}$ are determined by applying the Gauss-Legendre integration rule,

$$F_{t,k}^T = L_k \int_0^1 w_t(\xi_k) N(\xi_k) d\xi_k = L_k \sum_j \varsigma_j \left(w_t(\xi_{k,j}) N(\xi_{k,j}) \right). \tag{4.25}$$

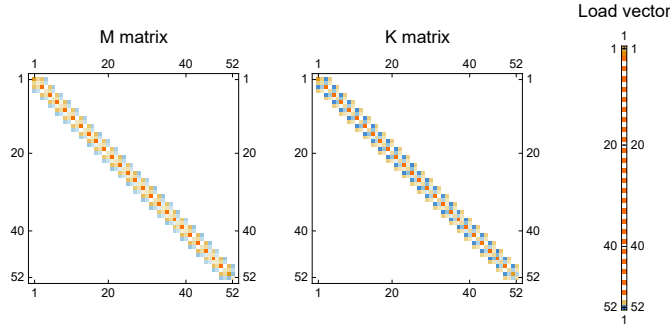


FIGURE 4.3: The mass (M), stiffness (K) and load Finite Element matrices/vector for $N = 25$ elements. The damping matrix (C) is a linear combination of the two matrices. Red to yellow indicate positive values, while blue indicates negative values. White indicates a zero value.

with $\varsigma_1 = \varsigma_2 = 1/2$, $\xi_{k,1} = (1 - \sqrt{1/3})/2$ and $\xi_{k,2} = (1 + \sqrt{1/3})/2$, and $F_t^\top = \sum_k F_{t,k}^\top P_k$. For a constant-valued distributed load function $w_t(x) = W_t$, each $F_{t,k}$ has the form $F_{t,k}^\top = W_t (1/2, L_k/12, 1/2, -L_k/12)$. The second and fourth value of $F_{t,k}$ may cancel out when the $F_{t,k}$ are summed for all elements and the L_k are equal for each element.

4.1.6 Overview

Using the derivations of Section 4.1.1 until Section 4.1.5 the integral minimization problem (2.6) is transformed into a finite-dimensional non-linear minimization problem which can be solved using linear algebra solvers and by making use of the Newton method.

Using each of the derivations, the minimization problem (2.6) can be transformed like

$$\begin{aligned} \min_y \int_0^L \frac{1}{2} EI (y'')^2 + \frac{1}{2} \mu \dot{y}^2 - wy + \Xi(d_N(y)) dx \\ \approx \min_q \frac{1}{2} \dot{q}_t^\top M \dot{q}_t + \frac{1}{2} q_t^\top K q_t - F_t^\top q_t + \sum_{j=1}^2 \varsigma_j \sum_k L_k \Xi \left(N(\xi_{k,j}) P_k q_t - f(\xi_{k,j}) \right) \end{aligned} \quad (4.26)$$

with a solution given by the equation in terms of q :

$$M \ddot{q}_t + C \dot{q}_t + K q_t + \sum_{j=1}^2 \varsigma_j A_j V_j(q_t) = F_t. \quad (4.27)$$

This is a non-linear equation because of the V_j terms, which in turn can be solved with Newton iterations. The iterations require the second derivative of the integral involving $J_j(q)$ as determined in (4.21). In fig. 4.3 a visualization of the stiffness, mass and load matrices/vector is given.

For the dynamic problem equation (4.27) describes the motion of the beam. This motion changes over time and this is solved by the integration step in Section 4.1.7. For the static problem, the terms \ddot{y} and \dot{y} are not present, which leaves a single non-linear equation which can be solved with the Newton method.

4.1.7 Numerical integration

The numerical integration of the dynamic problem is done using the Hilber-Hughes-Taylor- α (HHT- α) method [18]¹. This method has been chosen from a set of methods as found in [19] due to its implicitness and possibilities to reduce high-frequency oscillations which may occur in the solution process. Also, this method has proven to be effective in the research of Frans de Vries which makes it well applicable to related research.

The HHT- α method is based on the Newmark- β numerical integration method [20]. The assumptions will be listed, and using those assumptions the update rules used in the integration steps will be determined. The

¹In addition to [18], an unpublished document of Frans de Vries has also been used as reference. Contact: <https://www.utwente.nl/en/et/ms3/research-chairs/nsm/people/phdpd/FHdeVries>, f.h.devries@utwente.nl.

result will be a non-linear equation which can be solved using the Newton method. The Newton steps will also be determined explicitly for implementation purposes.

The goal of the integration step is integrating the equation of motion (4.27) for a time difference τ step. Given are the solution y_t and \dot{y}_t at time t , and after one step of integration the result is the solution $y_{t+\tau}$ and $\dot{y}_{t+\tau}$ at time $t + \tau$. Concretely, we wish to find $y_{t+\tau}$, $\dot{y}_{t+\tau}$ and $\ddot{y}_{t+\tau}$ satisfying the differential equation

$$M\ddot{y}_{t+\tau} + C\dot{y}_{t+\tau} + Ky_{t+\tau} + \sum_{j=1}^2 \zeta_j A_j \left(V_j(y_{t+\tau}) + V_j(\dot{y}_{t+\tau}) \right) = F_{t+\tau} \quad (4.28)$$

with V_j a (possibly non-linear) function, given $M, C, K, \zeta_j, A_j, V_j, F_t, F_{t+\tau}, y_t, \dot{y}_t$ and \ddot{y}_t .

The Newmark- β method and the HHT- α method give the assumptions required for the integration step. The Newmark- β method describes the relations between the deflection y , the velocity \dot{y} and the acceleration \ddot{y} at time t and $t + \tau$, namely

$$y_{t+\tau} = y_t + \tau \dot{y}_t + \frac{1}{2} \tau^2 \left((1 - 2\beta) \ddot{y}_t + 2\beta \ddot{y}_{t+\tau} \right), \quad (4.29)$$

$$\dot{y}_{t+\tau} = \dot{y}_t + \tau \left((1 - \gamma) \ddot{y}_t + \gamma \ddot{y}_{t+\tau} \right). \quad (4.30)$$

Furthermore the HHT- α method solves the equation

$$M\ddot{y}_{t+\tau} + C((1 - \alpha)\dot{y}_{t+\tau} + \alpha\dot{y}_t) + K((1 - \alpha)y_{t+\tau} + \alpha y_t) + \sum_{j=1}^2 \zeta_j A_j \left(V_j((1 - \alpha)y_{t+\tau} + \alpha y_t) + V_j((1 - \alpha)\dot{y}_{t+\tau} + \alpha\dot{y}_t) \right) = (1 - \alpha)F_{t+\tau} + \alpha F_t \quad (4.31)$$

instead of (4.28). Finally, the combination of the Newmark- β method and the HHT- α method assumes

$$\alpha \in \left[0, \frac{1}{3} \right], \quad \beta = \frac{1}{4} (1 + \alpha)^2, \quad \gamma = \frac{1}{2} + \alpha \quad (4.32)$$

to get second order unconditional stability.

With these assumptions, equations (4.29), (4.30) and (4.32) are substituted into the expression (4.31) leading to the non-linear equation

$$\begin{aligned} 0 &= M\ddot{y}_{t+\tau} + C((1 - \alpha)\dot{y}_{t+\tau} + \alpha\dot{y}_t) + K(\alpha y_t + (1 - \alpha)y_{t+\tau}) \\ &\quad + \sum_{j=1}^2 \zeta_j A_j \left(V_j((1 - \alpha)y_{t+\tau} + \alpha y_t) + V_j((1 - \alpha)\dot{y}_{t+\tau} + \alpha\dot{y}_t) \right) - \alpha F_t - (1 - \alpha)F_{t+\tau} \\ &=: G(y_{t+\tau}) \end{aligned} \quad (4.33)$$

of only one unknown variable $y_{t+\tau}$, since (see (4.29), (4.30) and (4.32))

$$\dot{y}_{t+\tau} = \frac{\ddot{y}_t \alpha^2 \tau^2 + ((\alpha - 2)\alpha - 1)\tau \dot{y}_t - 2(2\alpha + 1)(y_t - y_{t+\tau})}{(\alpha + 1)^2 \tau}, \quad (4.34)$$

$$\ddot{y}_{t+\tau} = \ddot{y}_t - \frac{2(\ddot{y}_t \tau^2 + 2(\tau \dot{y}_t + y_t - y_{t+\tau}))}{(\alpha + 1)^2 \tau^2}. \quad (4.35)$$

Finally (4.33) is solved with the Newton method because the resulting equation is non-linear. A single Newton iteration is given by

$$y_{t+\tau}^{(k+1)} = y_{t+\tau}^{(k)} - \left(\nabla G(y_{t+\tau}^{(k)}) \right)^{-1} G(y_{t+\tau}^{(k)}) \quad (4.36)$$

with $y_{t+\tau}^{(0)} = y_t$. The expression for $\nabla G(y_{t+\tau}^{(k)})$ can be found to be

$$(1 - \alpha)K + \frac{2(1 - \alpha)(1 + 2\alpha)}{(\alpha + 1)^2 \tau} C + \frac{4}{(\alpha + 1)^2 \tau^2} M + \sum_{j=1}^2 \zeta_j A_j \left((1 - \alpha)J_j(y_{t+\tau}^{(k)}) + \frac{2(1 - \alpha)(2\alpha + 1)}{(\alpha + 1)^2 \tau} J_j(\dot{y}_{t+\tau}^{(k)}) \right) A_j^T \quad (4.37)$$

where $y_{t+\tau}^{(k)}$ is calculated using (4.34) but using the value of $y_{t+\tau}^{(k)}$ for $y_{t+\tau}$.

The parameter α can be used to control the numerical damping of the HTT- α method. This is useful in situations where high-frequency oscillations may occur due to numerical integration, which may be the case when integrating the dynamic beam problem for a long timespan and large time steps. See Section 6.2.2 for an example of such a situation.

4.2 Reference solution

This section concerns a special case of Equation (2.13), using specified boundary conditions, no distributed load but including contact. For this problem, an analytic solution can and has been determined of the equilibrium (static problem). This analytic solution is used later in Chapter 6 for measuring the accuracy and convergence of a numerical solution. It is therefore dubbed the *reference solution* and is denoted with $y_{\text{ref}}(x)$.

In order to find the reference solution, the static beam problem (2.13) is solved with the boundary conditions, but with a variable length $L = \hat{L}$. The extra variable \hat{L} is introduced to satisfy the contact constraint of the solution. Thus we can find a general solution $y_{\hat{L}}(x)$ in terms of \hat{L} , after which the value of \hat{L} can be adjusted such that an extra constraint (contact) is enforced. The reference solution is then extended to form a solution for the entire length of the beam. Concretely, we solve

$$EI y_{\hat{L}}'''' = 0 \quad (4.38)$$

subject to

$$y_{\hat{L}}(0) = y_0, \quad y_{\hat{L}}'(0) = \vartheta_0, \quad y_{\hat{L}}(\hat{L}) = 0, \quad y_{\hat{L}}'(\hat{L}) = 0 \quad (4.39)$$

with $y_0 > 0$ and $\vartheta_0 < 0$. This problem has the explicit solution

$$y_{\hat{L}}(x) = y_0 + \vartheta_0 x + \left(-\frac{3}{\hat{L}^2} y_0 - \frac{2}{\hat{L}} \vartheta_0 \right) x^2 + \left(\frac{2}{\hat{L}^3} y_0 + \frac{1}{\hat{L}^2} \vartheta_0 \right) x^3. \quad (4.40)$$

The extra constraint that contact is satisfied, is given by the requirement that $y_{\hat{L}}''(\hat{L}) = 0$. This means that there is no force on the solution at $x = \hat{L}$, the point of contact. This extra condition is satisfied for $\hat{L} = -3(y_0/\vartheta_0)$. So, concretely, if we substitute the values of y_0 , ϑ_0 and \hat{L} into (4.40) and extend the domain to $[0, L]$ we find the reference solution y_{ref} given by

$$y_{\text{ref}}(x) = \begin{cases} y_{\hat{L}}(x) & 0 \leq x < \hat{L} \\ 0 & \hat{L} \leq x \leq L \end{cases} = \begin{cases} \frac{\vartheta_0^3 x^3}{27 y_0^2} + \frac{\vartheta_0^2 x^2}{3 y_0} + \vartheta_0 x + y_0 & 0 \leq x < -\frac{3 y_0}{\vartheta_0} \\ 0 & -\frac{3 y_0}{\vartheta_0} \leq x \leq L \end{cases}. \quad (4.41)$$

See fig. 4.4 for a visualization with $y_0 = 1$ and $\vartheta_0 = -1/2$. Thus, the *reference distance* of a Finite Element solution is given by the distance between the solution y_t and the reference solution,

$$\int_0^L (y_t(x) - y_{\text{ref}}(x))^2 dx \approx \sum_{k=1}^N \sum_{j=1}^2 \varsigma_j \left(y_t(\xi_{k,j}) - y_{\text{ref}}(\xi_{k,j}) \right)^2. \quad (4.42)$$

where the integral is approximated with the Gauss Legendre approximation introduced in Section 4.1.4 and the $\xi_{k,j}$ are the integration points for element-local coordinates. Notice that better approximations can be found (for example including the values of ϑ_k), but the current expression works well enough for performing a convergence analysis.

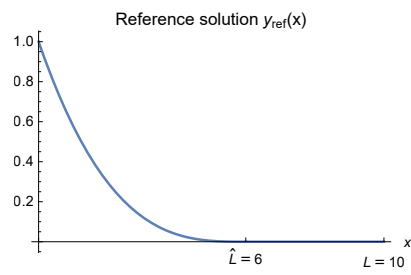


FIGURE 4.4: Reference solution of Finite Element method with $y_0 = 1$, $\vartheta_0 = -1/2$ and $L = 10$.

Chapter 5

Analysis: Simplification of middle section

The aim of this chapter is to provide a simplification of the model presented in Chapter 2, for the section which has no contact. Instead of simulating a solution with a numeric solver using the Finite Element method as presented in Chapter 4, the middle section of the pipe can be analyzed using system theory and approximated using a simplified version of the transfer function of the system dynamics.

Using this simplification, simulations can be run for the part of the pipe on the stinger which requires complex contact simulations and for the part which makes contact with the seabed, and the two sub-problems can be ‘connected’ via the transfer functions determined in this chapter. A further simplification for the contact with the seabed can be found in the results, see Section 7.2.

5.1 Laplace domain

Instead of solving the entire partial differential equation found in (2.11), we instead analyze the equation in the Laplace domain. This allows us to eliminate the temporal variable t by replacing it with a frequency parameter s . By treating s as a parameter instead of a variable, the resulting equation is an ordinary differential equation which can be solved analytically and will result in the transfer function.¹

Equation (2.11) without a distributed load is given by

$$EIy''''(t, x) + c_d \dot{y}(t, x) + \mu \ddot{y}(t, x) = 0 \quad (5.1)$$

with some boundary and initial conditions. Equation (5.1) can be extended to include a more extended model or distributed load, but the current model already gives rise to difficult equations. In case of a non-linear partial differential equation, the following steps in this chapter become more involved and may not be possible.

All of the eight possible boundary conditions of (5.1) are identified with a function $u_i(t)$, $i \in \{1, \dots, 8\}$, like

$$\begin{aligned} y(t, 0) &= u_1(t), & y'(t, 0) &= u_2(t), & EIy''(t, 0) &= u_3(t), & EIy'''(t, 0) &= u_4(t), \\ y(t, L) &= u_5(t), & y'(t, L) &= u_6(t), & EIy''(t, L) &= u_7(t), & EIy'''(t, L) &= u_8(t). \end{aligned} \quad (5.2)$$

Four of the u_i are known and can be considered as boundary inputs for the dynamic system. The other four u_i are considered output functions and can be analyzed using the transfer function which will be determined.

The time domain is transformed to the Laplace domain, transferring $y(t, x)$ to $Y(s; x)$ and all $u_i(t)$ to $U_i(s)$ for $i \in \{1, \dots, 8\}$. We get the Laplace domain form of (5.1) as

$$EIY''''(s; x) + c_d s Y(s; x) + \mu s^2 Y(s; x) = 0 \quad (5.3)$$

with the similarly transformed boundary input and output functions

$$\begin{aligned} Y(s; 0) &= U_1(s), & Y'(s; 0) &= U_2(s), & EIY''(s; 0) &= U_3(s), & EIY'''(s; 0) &= U_4(s), \\ Y(s; L) &= U_5(s), & Y'(s; L) &= U_6(s), & EIY''(s; L) &= U_7(s), & EIY'''(s; L) &= U_8(s). \end{aligned} \quad (5.4)$$

¹It is also possible to do this in a slightly longer way by following the steps in [21]. First the entire spatial solution of the partial differential equation can be solved (with time-dependent boundary conditions). Then a set of ordinary differential equations can be Laplace transformed and solved in order to find a transfer function.

Notice the temporal derivatives in (5.3) which have been associated with powers of s .

We can choose different combinations of boundary conditions in order to solve the differential equation (5.3) and determine a transfer function for a chosen input and output function. For example, if the functions U_1 , U_2 , U_7 and U_8 are assumed to be known, then the equation can be solved for $Y(s; x)$ under these boundary conditions. With the aid of MATHEMATICA the solution is found to have the (monstrous) form

$$Y(s; x) = \frac{Y_1(s; x)}{Z(s)} U_1(s) + \frac{Y_2(s; x)}{Z(s) \sqrt[4]{-s(c_d + \mu s)}} U_2(s) + \frac{Y_3(s; x)}{Z(s) \sqrt{-EI s(c_d + \mu s)}} U_7(s) + \frac{Y_4(s; x)}{Z(s) \sqrt[4]{-EI (s(c_d + \mu s))^3}} U_8(s) \quad (5.5)$$

with

$$\begin{aligned} Z(s) &= 2 \left((e^{\beta_1} + 1) (1 + e^{2i\beta_2 L}) + 4e^{(1+i)\beta_2 L} \right) \\ Y_1(s; x) &= e^{(-1-i)\beta_2 x} \left(e^{\beta_1} \left((1-i)e^{i\beta_2(2L+x)} + e^{\beta_2(x+2iL)} + e^{(1+2i)\beta_2 x} + (1+i)e^{i\beta_2 x} \right) + 2e^{\beta_2(x+(1+i)L)} + 2e^{\beta_2((1+i)L+ix)} \right. \\ &\quad \left. + 2e^{\beta_2((1+i)L+(2+i)x)} - ie^{\beta_2(2L+(1+2i)x)} + 2e^{\beta_2((1+i)L+(1+2i)x)} + (1-i)e^{\beta_2(x+2iL)} + ie^{\beta_2(x+(2+2i)L)} \right. \\ &\quad \left. + (1+i)e^{\beta_2(2iL+(2+i)x)} + (1-i)e^{(2+i)\beta_2 x} + (1+i)e^{(1+2i)\beta_2 x} \right) \\ Y_2(s; x) &= \sqrt[4]{EI} e^{\beta_2(-(x+iL)} \left(-2e^{(1+2i)\beta_2 L} + e^{\beta_1} \left((-1+i)e^{i\beta_2 L} - (1+i)e^{3i\beta_2 L} + e^{\beta_2(3iL+(1-i)x)} + e^{\beta_2(iL+(1+i)x)} \right) \right. \\ &\quad \left. + 2e^{\beta_2(2x+(1+2i)L)} - (1-i)e^{\beta_2(3iL+(1-i)x)} - (1+i)e^{\beta_2(iL+(1+i)x)} - ie^{\beta_2((2+i)L+(1+i)x)} - 2ie^{\beta_2((1+2i)L+(1+i)x)} \right. \\ &\quad \left. + (1-i)e^{\beta_2(2x+3iL)} + 2ie^{\beta_2((1+2i)L+(1-i)x)} + ie^{\beta_2((2+3i)L+(1-i)x)} + (1+i)e^{\beta_2(2x+iL)} \right) \\ Y_3(s; x) &= e^{\beta_2(-(x+iL)} \left(2e^{\beta_1+2i\beta_2 L} + (1+i) \left(e^{(1+3i)\beta_2 L} + (-i)e^{(1+i)\beta_2 L} + (1-i) \left(-e^{(1+i)\beta_2(L+x)} \right) + (1-i)e^{2\beta_2(x+iL)} \right. \right. \\ &\quad \left. \left. - (1-i)e^{\beta_2((1+3i)L+(1-i)x)} - e^{(1+i)\beta_2(2L+x)} - ie^{\beta_2(2x+(1+3i)L)} - e^{\beta_2(2iL+(1-i)x)} + e^{2\beta_2 x+(1+i)\beta_2 L} + \right. \right. \\ &\quad \left. \left. ie^{(1+i)\beta_2(x+(1+i)L)} + ie^{(1+i)\beta_2(2L-ix)} \right) \right) \\ Y_4(s; x) &= e^{\beta_2(-(x+iL)} \left((1+i) \left(-e^{(1+i)\beta_2 L} + ie^{(1+3i)\beta_2 L} + (1-i)e^{2\beta_2(x+iL)} + e^{(1+i)\beta_2(2L+x)} + e^{\beta_2(2x+(1+3i)L)} \right. \right. \\ &\quad \left. \left. - e^{\beta_2(2iL+(1-i)x)} - (1+i)e^{\beta_2((1+3i)L+(1-i)x)} - ie^{(1+i)\beta_2(2L-ix)} - ie^{2\beta_2 x+(1+i)\beta_2 L} + ie^{(1+i)\beta_2(x+(1+i)L)} \right. \right. \\ &\quad \left. \left. + (1+i)e^{(1+i)\beta_2(L+x)} \right) - 2e^{\beta_1+2i\beta_2 L} \right) \end{aligned} \quad (5.6)$$

and

$$\beta_1 = 2L\beta_2, \quad \beta_2^4 = \frac{-s(c_d + \mu s)}{EI}. \quad (5.7)$$

Notice that β_2 can be determined using any of the four solutions of equation (5.7) because all solutions give the same function. While it is cumbersome to check for the expression in (5.5), the it is far easier to see in the following example.

In case we are interested in the transfer function from U_2 (the angle at $x = 0$) to U_5 (the deflection at $x = L$) denoted by $H_{U_2 \rightarrow U_5}$, we can ignore the other U_i (i.e. set $U_1 = U_7 = U_8 = 0$), simplify the expression for $Y(s; x)$ and find

$$U_5(s) = Y(s; L) = \frac{1}{\beta_2} \frac{(\sin(L\beta_2) + \sinh(L\beta_2))}{(\cos(L\beta_2) \cosh(L\beta_2) + 1)} U_2(s) \quad (5.8)$$

which gives the transfer function

$$H_{U_2 \rightarrow U_5}(s) = \frac{1}{\beta_2} \frac{(\sin(L\beta_2) + \sinh(L\beta_2))}{(\cos(L\beta_2) \cosh(L\beta_2) + 1)}. \quad (5.9)$$

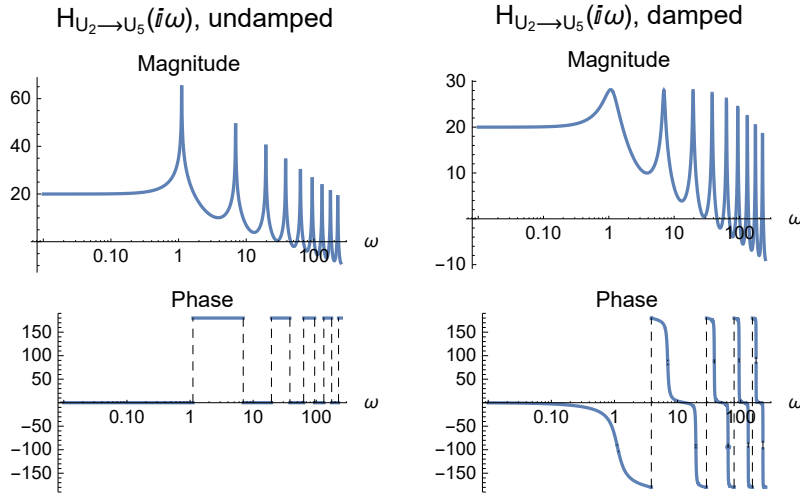


FIGURE 5.1: Bode plot of $H_{U_2 \rightarrow U_5}(i\omega)$ for $10^{-2} \leq \omega \leq 2.5 \times 10^2$ of the undamped ($c_d = 0$) and damped ($c_d = 5$) dynamic system.

A Bode plot of the transfer function for this example is given in fig. 5.1 for a non-damped and a damped system. The used parameters are $EI = 10^4$ [$\text{m}^4\text{N}/\text{m}^2 = \text{Nm}^2$], $\mu = 10^2$ [kg/m], $c_d \in \{0, 5\}$ [kg/ms] (respectively undamped and damped) and $L = 10$ [m]. Notice how the undamped system has a non-continuous phase with jumps at the poles of the transfer function. The damped system rather has a continuous phase and its poles have moved away from the imaginary axes, and the plot of the transfer function on the imaginary axes has been smoothed out.

In equation (5.9), the denominator contains the eigenvalue equation of the dynamic system (see fig. A.1) which will cause an infinite amount of poles which means that the transfer function cannot be represented by a rational function. This is true in general for transfer functions of this dynamical system, although the eigenvalue equation may be different for different combinations of boundary conditions. In Section 5.2 we approximate the transfer function with a rational function which transforms the behaviour of the dynamic system into that of a simpler system.

Of course this example is limited and the steps taken above can be repeated to find any of the transfer functions in the system. Furthermore, the inputs of the system can also be changed to for example U_1 , U_2 , U_5 and U_6 (the deflection and angle are known for both ends of the beam), or U_1 , U_3 , U_5 and U_7 (the deflection and curvature are known at both ends of the beam). Similar transfer functions can be determined in order to find the frequency response of the shear force or the moment at the ends of the beam.

5.2 Approximation of transfer function

In the above section the transfer function has been determined from an input function to an output function. It may be advisable to approximate this transfer function with a rational function (a fraction of two finite degree polynomials). An approximation is useful because the analytic transfer function has an infinite amount of non-trivial zeros. That may be difficult to work with if the dynamic system is part of a larger system or analysis is required where the poles and zeros must be known.

The main assumption which is used in the following approximations of the transfer function, is that the high frequencies do not matter in the solution. This means that the transfer function should match the one found analytically for the lower frequencies, and less so for the higher frequencies. This may cause the poles and zeros to move slightly, depending on the approximation method and the order of the approximation. In the case of pipelaying, any frequencies higher than 10 Hz are not interesting for the solution. After all, we are interested in the behaviour of the pipe, not high-frequency vibrations in the pipe. Of course the frequency range of interest can be adjusted depending on the problem requirements and parameters.

Three options are given here for approximating the analytic transfer function by a rational function. The first option involves the Taylor expansion while the other two options use the *Padé Approximant* [22]. In this thesis we will not go into great detail how to calculate the approximations, the reader is directed to the relevant literature.

Taylor approximation The first approximation is done using the Taylor approximation around $\beta_2 = 0$ of each individual term in (5.9), and then substituting . We use that

$$\begin{aligned}\sin(\xi) &= \lim_{N_A \rightarrow \infty} \sum_{k=0}^{N_A} (-1)^k \frac{\xi^{2k+1}}{(2k+1)!}, & \sinh(\xi) &= \lim_{N_A \rightarrow \infty} \sum_{k=0}^{N_A} \frac{\xi^{2k+1}}{(2k+1)!}, \\ \cos(\xi) &= \lim_{N_A \rightarrow \infty} \sum_{k=0}^{N_A} (-1)^k \frac{\xi^{2k}}{(2k)!}, & \cosh(\xi) &= \lim_{N_A \rightarrow \infty} \sum_{k=0}^{N_A} \frac{\xi^{2k}}{(2k)!}.\end{aligned}\quad (5.10)$$

However, instead of taking the limit, the sum is truncated at some finite value of N_A . For a Taylor approximation of the transfer function with the highest polynomial order of 8 in s , the approximation is represented by a rational function of order 2 (numerator) and 8 (denominator) in s given by

$$H_{U_2 \rightarrow U_5}(s) \approx 2.7095 \times 10^7 L \frac{\beta_2^4 L^4 + 120}{\beta_2^{16} L^{16} + 224 \beta_2^{12} L^{12} + 645120 \beta_2^8 L^8 - 2.7095 \times 10^8 \beta_2^4 L^4 + 3.2514 \times 10^9}.\quad (5.11)$$

Notice that even though the sin, cos, sinh and cosh Taylor approximations contain terms that are not powers of four, the resulting approximation only contains powers of four, making the transfer function approximation rational in s after substitution of β_2 .

Term Padé approximation For the Padé approximation of the transfer function, we are looking for a rational polynomial of β_2 of the form

$$\frac{\sum_{k=0}^{N_A} a_k \beta_2^k}{1 + \sum_{k=1}^{M_A} b_k \beta_2^k},\quad (5.12)$$

for some fixed values of N_A and M_A which approximates the required function. The substitution of β_2 in terms of s will be done afterwards.

As an example, we can take $N_A = M_A = 4$ (to get an 8 order approximation in s) and find the Padé approximations

$$\begin{aligned}\sin(\xi) &\approx -56.3636 \frac{\xi^3 - 9.48387\xi}{\xi^4 + 32.7273\xi^2 + 534.545}, & \sinh(\xi) &\approx 56.3636 \frac{\xi^3 + 9.48387\xi}{\xi^4 - 32.7273\xi^2 + 534.545}, \\ \cos(\xi) &\approx 24.0769 \frac{\xi^4 - 22.0447\xi^2 + 48.3067}{\xi^4 + 50.7692\xi^2 + 1163.08}, & \cosh(\xi) &\approx 24.0769 \frac{\xi^4 + 22.0447\xi^2 + 48.3067}{\xi^4 - 50.7692\xi^2 + 1163.08}.\end{aligned}\quad (5.13)$$

Even though non-fourth powers occur in the approximating terms, they cancel out when combined into the transfer function, resulting in a rational transfer function in s . The term Padé approximation of the transfer function is given by

$$H_{U_2 \rightarrow U_5}(s) \approx \frac{\beta_2^4 L^5 \left(8.19418 \beta_2^8 L^8 - 1075.58 \beta_2^4 L^4 + 1.08373 \times 10^7 \right) + 1.33127 \times 10^9 L}{-1.11196 \times 10^8 \beta_2^4 L^4 + \beta_2^8 L^8 \left(\beta_2^8 L^8 - 391.102 \beta_2^4 L^4 + 291170 \right) + 1.33127 \times 10^9}.\quad (5.14)$$

Again, notice that only powers which are a multiple of four occur in the approximation, making the approximation rational in s .

Function Padé approximation Furthermore, it is also possible to take the expression in (5.9) and find a Padé approximation at once for the entire expression. This will become

$$H_{U_2 \rightarrow U_5}(s) \approx 0.00252093 \frac{\beta_2^{16} L^{17} + 29576.5 \beta_2^{12} L^{13} + 3.39367 \times 10^8 \beta_2^8 L^9 + 9.236 \times 10^{11} \beta_2^4 L^5 + 1.10323 \times 10^{14} L}{\beta_2^{16} L^{16} - 16464.3 \beta_2^{12} L^{12} + 5.42916 \times 10^7 \beta_2^8 L^8 - 2.31658 \times 10^{10} \beta_2^4 L^4 + 2.78118 \times 10^{11}}\quad (5.15)$$

a representation of only powers which are a multiple of four and hence a rational function of order 8 in s after substitution of β_2 .

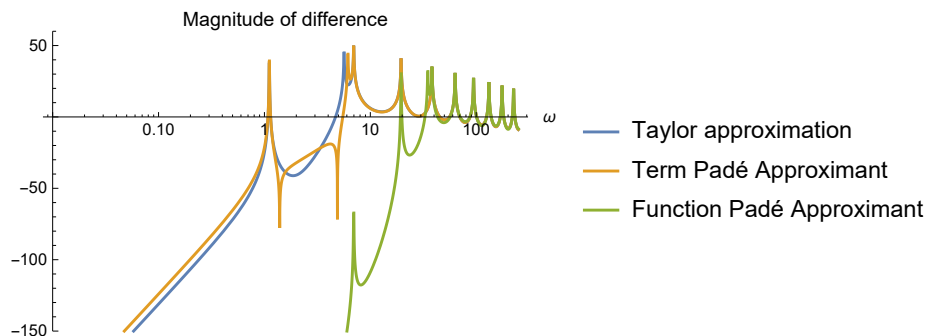


FIGURE 5.2: Bode magnitude plot of the undamped system with a the three order 8 approximations of the transfer function compared to the analytic transfer function.

In fig. 5.2 the Taylor and Padé order 8 approximations are compared with the analytic form (5.9) in a Bode magnitude plot of the undamped example problem given in Section 5.1. The per-term Padé approximation works better than the Taylor approximation, but the function Padé approximation gives the best order 8 approximation for this example. There are undoubtedly better methods for approximating the transfer function, but these three methods (Taylor and term- and function Padé approximation) give a good basis that works well for transfer functions will only a few poles in the frequency range of interest.

Chapter 6

Results

6.1 Implementation

The modelling assumptions, deductions and numerical methods have been implemented using the software package WOLFRAM MATHEMATICA. This software is useful for rapid prototyping of mathematical and numerical techniques. Not only does the package contain many built-in numerical procedures, it also allows calculating and solving symbolic equations and problems. Furthermore, the results can be visualized in many different forms which gives more insight in the generated data and results.

Of course, the results presented in this research can be implemented more efficiently in a low-level (compiled) programming language in order to get better performance for large calculations.

6.1.1 Verification of implementation

In order to give the results presented later in this chapter any validity, a verification of the implementation has been performed for multiple different aspects: the solution shape for a static problem and the solution shape and vibration frequencies for the dynamic problem.

Static problem

The static problem (2.13) has been solved with the Finite Element implementation without any contact enforced. The boundary conditions have been taken as

$$y(0) = y_0, \quad y'(0) = \vartheta_0 \quad EIy''(L) = 0, \quad EIy'''(L) = 0 \quad (6.1)$$

and a distributed load $w = \gamma x^3$. The exact solution to this problem is

$$y(x) = \frac{\gamma x^2}{840EI} (84L^5 - 35L^4 x + x^5) + \vartheta_0 x + y_0 \quad (6.2)$$

and for the values $y_0 = 1$ m, $\vartheta_0 = -1/2$, $EI = 10^4$ [N/m²], $L = 10$ [m], $\gamma = 5/100$ and $N = 25$ elements, we get a Finite Element numerical solution which matches the exact solution almost perfectly (see fig. 6.1).

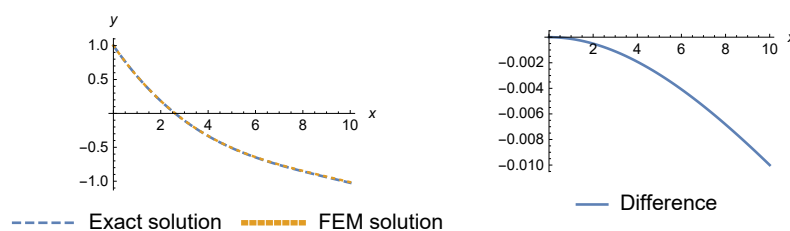
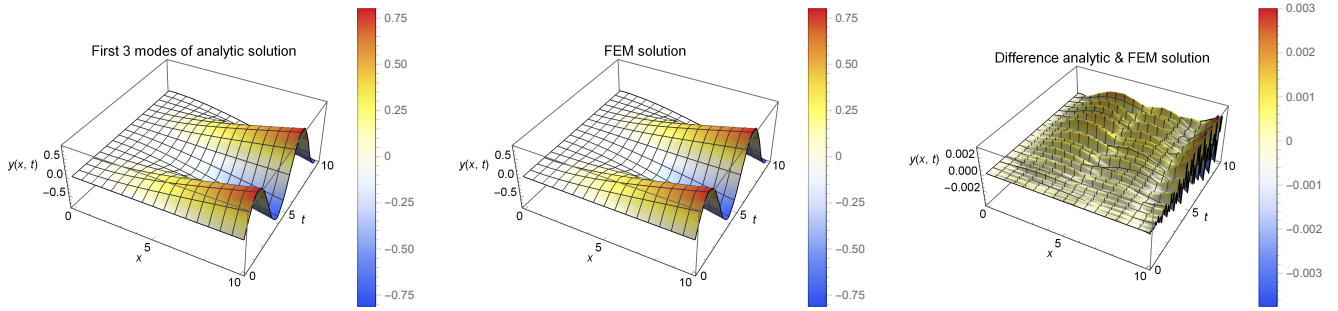


FIGURE 6.1: Comparison a static analytical and numerical (Finite Element) solution with distributed load.


 FIGURE 6.2: Analytical and Finite Element solution and their difference. Notice the scale of the y axis in the last plot.

Dynamic problem

For the dynamic problem, several verifications have been performed. The dynamic problem of a simple clamped beam (cantilever beam) is considered, with no distributed load or damping. The analytical eigenvalues are compared with those of the numerical solution, calculated in two different ways. Furthermore, the entire solution over a small time domain is compared numerically.

The problem in (2.11) is solved with $w = 0$ and $c_d = 0$ and homogeneous boundary conditions given by

$$y(t, 0) = 0, \quad y'(t, 0) = 0, \quad EIy''(t, L) = 0, \quad EIy'''(t, L) = 0. \quad (6.3)$$

In Appendix A.2 the derivation of the analytical solution can be found. Its form is

$$y(t, x) = \sum_n (F_n \sin(\omega_n t) + G_n \cos(\omega_n t)) \left((\sin(\nu_n x) - \sinh(\nu_n x)) + B (\cos(\nu_n x) - \cosh(\nu_n x)) \right). \quad (6.4)$$

with $B = (\sin(\nu_n L) + \sinh(\nu_n L)) / (\cos(\nu_n L) + \cosh(\nu_n L))$. For the constants $EI = 10^4$ [Nm²], $\mu = 10$ [kg/m] and $L = 10$ [m] the first numerical values of $\nu_n L$ given by

$$\nu_1 L \approx 1.8751 \quad \nu_2 L \approx 4.69409 \quad \nu_3 L \approx 7.85476 \quad \nu_4 L \approx 10.9955 \quad (6.5)$$

and $\omega_n^2 = (EI/\mu)\nu_n^4$ which causes the first values of ω_n to be

$$\omega_1 \approx 1.11186 \quad \omega_2 \approx 6.96848 \quad \omega_3 \approx 19.5222 \quad \omega_4 \approx 38.3182. \quad (6.6)$$

We impose the initial conditions $y_0(x) = 0$ and $v_0(x) = (x/L)^2$ and then the first few numerical values of F_n can be found to be

$$F_1 \approx 0.294062 \quad F_2 \approx -0.005757, \quad F_3 \approx 0.000422398 \quad F_4 \approx -0.0000787057. \quad (6.7)$$

and the constants $G_n = 0$ for all n . The values of F_n decay as $1/n$, although it is difficult to find an analytic representation of the values. The analytical solution, the Finite Element solution and their difference is given in fig. 6.2. The time step $\tau = 0.025$ [s/step], the simulated time is $T = 10$ [s], $N = 8$ elements are used and the HHT- α parameter $\alpha = 0$. The analytical and the Finite Element solution coincide well which validates the dynamics of the numerical implementation. The quick convergence of the Finite Element solution to the analytical solution is due to the initial condition that is close to a linear combination of the first three basis functions.

In order to validate the values of the natural frequencies of the beam, two methods have been used. The first method is easier and is presented here. The second method is more elaborate and can be found in Appendix A.3.

The Finite Element discretization gives a linear system of equations, as found in Section 4.1.6 where the matrices K and M have the boundary conditions $y(0) = 0$ and $y'(0) = 0$ enforced. The values of α_1 and α_2 are taken as zero which removes all damping. By analyzing solutions of the form $q_0 e^{i\omega t}$ for some non-zero vector q_0 . Then derivation with respect to time can be evaluated and the resulting equations are

$$-Mq_0 e^{i\omega t} \omega^2 + Kq_0 e^{i\omega t} = 0 \quad (6.8)$$

which is a generalized eigenvalues equation. It can be solved efficiently numerically and the first few numerical results for $N = 8$ elements are

$$\omega_1 \approx 1.11186 \quad \omega_2 \approx 6.96848 \quad \omega_3 \approx 19.5222 \quad \omega_4 \approx 38.3182. \quad (6.9)$$

which match the analytical values in (6.6) perfectly for the the number of significant digits, although one digit after the significant part the values differ from those in (6.6). These values also correspond to similar results found in [23].

6.2 Contact

This section shows the characteristics and behaviour of the numerical solutions using the contact methods presented in Chapter 3. First the static problem with specific boundary conditions is considered and then the dynamic problem with similar boundary conditions. Several things are interesting for both situations, namely the convergence to the required solution (the reference solution), the violation of the contact surface and the manner of convergence (linear or quadratic). Because the Newton method is used to solve the non-linear equations, a quadratic convergence is not guaranteed. The solving speed of an iteration is not considered because this is not a point of interest in the current implementation.

6.2.1 Static problem

For the static problem a number of different things can be compared in the solution. We look at the number of elements, number of Newton iterations per update of p , the update scheme for p and the Newton convergence.

To compare the static methods, the problem is taken as (2.13) with boundary conditions

$$y(0) = 1, \quad y'(0) = -1/2, \quad EIy''(L) = 0 \quad EIy'''(L) = 0. \quad (6.10)$$

Contact is imposed at the surface $y = 0$ with the constraint $y(x) \geq 0$ for all x in a valid solution. This means that $d_N(y) = y$, and d_N is the identity operator. This problem has the reference solution $y_{\text{ref}}(x)$ as its exact solution. The used parameters for simulating the static problem are $EI = 10^4$ [Nm²], $\mu = 10$ [kg/m] and $L = 10$ [m]. The number of finite Element elements and the values of the penalty parameter are indicated per contact method. The Newton iterations are considered converged if either the Newton step size is less than $\varepsilon = 10^{-5}$ or 10 iterations have been made (whichever happens first).

Explanation for interpretation of the plots: For each of the following paragraphs, references to plots of solutions of the static problem will be made. In each of the figures the same kind of plots will be shown for each solution. The leftmost plot contains the solutions $y(x)$ for each problem or iteration of the solution method. A plot of the values of $\lambda(x)$ is shown, for each problem or iteration of the solution method, if applicable. Then a (logarithmic-scaled) convergence plot is shown of the reference distance and contact violation norm. Finally, a convergence plot is shown for each problem. For each problem or iteration of the contact method, some number of Newton iterations are made. For each iteration, the Newton step size is shown as a •. Furthermore, for each time step the total number of Newton iterations is indicated with a label at the last •. If this number is large or the •'s are close together, there is bad convergence.

Penalty method Simulation results using the Penalty method with both $N = 8$ elements and $N = 25$ elements are given in fig. 6.3. The problem (6.10) has been solved four times for each number of elements, each time with a different value of p . There are no iterations in the Penalty method apart from the Newton method, so the value of p is not updated throughout the solution process. Although the number of Newton iterations changes slightly, even using $N = 8$ elements is more than enough to converge well to the solution with contact enforced. The linear convergence to the reference solution is equal for both number of elements.

For each of the problems with different values of p a quadratic Newton convergence can be observed, which is important for finding a quick solution in case of larger problems. Note that for $p = 10^2$, the solution itself is not good because contact is not enforced well. In contrast, using $p = 10^5$ gives a solution which lies nicely on the contact surface $f(x) = 0$.

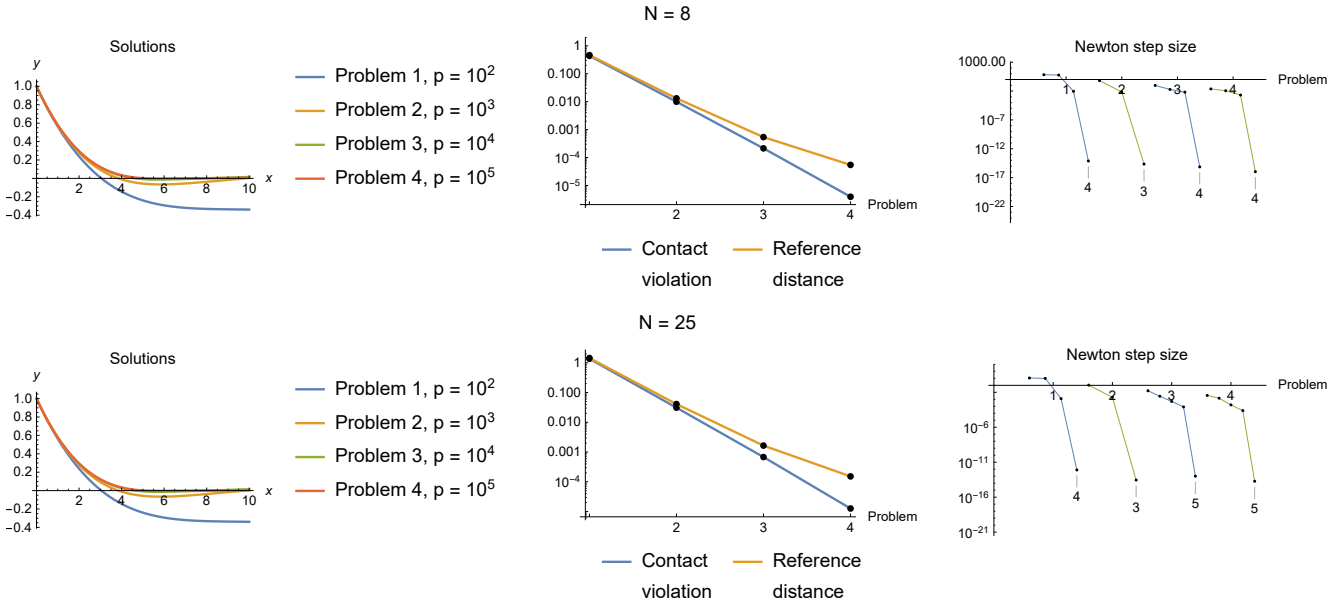


FIGURE 6.3: Four solutions of the static problem with a convergence plot and the Newton step sizes, using $N = 8$ and $N = 25$ elements.

Augmented Lagrangian method The Augmented Lagrangian method has been employed to find its performance and look into its Newton convergence. For updating the value of p , the parameters $p_0 = 10^2$ and $\psi \in \{1, 4\}$ have been used which correspond to $p = p_0 = 10^2$ ($\psi = 1$) and increasing values of p ($\psi = 4$). Five iterations of a single problem have been solved. The results are given in fig. 6.4.

It can be observed that using $\psi = 1$ the solution converges to a solution, but with only some contact enforced. If this is compared to the solution of $p = 10^2$ using the Penalty method, one can see that there is less contact violation. Also, mostly quadratic convergence can be seen in the Newton convergence plots, although the last few iterations make it hard to distinguish linear from quadratic convergence.

Using $\psi = 4$ a better solution can be seen, although the convergence to that solution is more ‘wild’. Furthermore, the contact violation is often non-existent because the solution does not violate the contact surface. Finally, the Newton convergence takes more steps to reach a converged state per iteration, but at step $k = 4$ a linear convergence can be seen. This behaviour sometimes takes place when using the Augmented Lagrangian method but only for a single step. It may be an interesting point for future analysis of the method to see under what conditions the convergence changes from quadratic to linear.

Augmented Barrier method In fig. 6.5 the results of solving the static problem using the Augmented Barrier method can be found.

Different values for η are compared using the Augmented Barrier method with $\psi = 2.5$, to see if it makes sense to take a weighted average of the current and the new value of λ in the λ update step. For $\eta = 1$, which ignores λ altogether, a slow convergence of the solution can be seen. For $\eta = 1/2$, an average in the usual sense of the current and the updated value of λ , a good decrease of the contact violation is observed and a very small increase in the quality of the solution (the reference distance). However, it takes more Newton steps to reach that solution in comparison to the situation with $\eta = 0$. Because there is no apparent improvement numerically to use the $\eta \neq 0$ weighing parameter in the λ update step we conclude that $\eta = 0$ will be used.

Furthermore, different values of ψ are compared. Using $\psi = 1$, the solution converges to a fixed reference distance, although the solution is both better than the Penalty and Augmented Lagrangian solution for $p_0 = 10^2$ (and $\psi = 1$ in case of the Augmented Lagrangian method). However, for $\psi = 2.5$ the solution converges steadily to the reference solution. In contrast we can see $\psi = 4$ which also converges well, but not quicker or steadier (notice the missing contact violation at step $k = 4$ and the increase in Newton steps for each step). It must be noted that choosing the specific value of ψ is dependent on the problem. Convergence must always be checked well before fixing parameters.

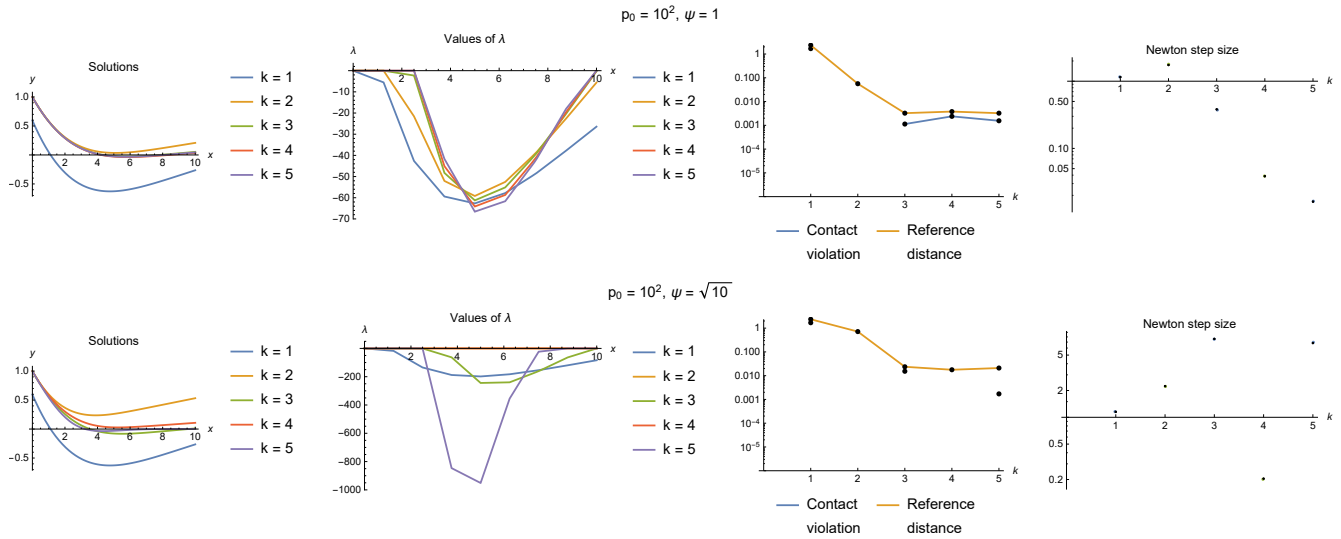


FIGURE 6.4: The solution of the static problem with the value of λ , a convergence plot and the Newton step sizes, using $p_0 = 10^2$ and $\psi \in \{1, 4\}$.

6.2.2 Dynamic problem

The used parameters for simulations of the dynamic problem are $EI = 10^4$ [Nm²], $\mu = 10$ [kg/m] and $L = 10$ [m], $\tau = 0.1$ [s/step], $T = 6$ [s] and $\alpha = 0.01$. The number of Finite Elements is $N = 12$. The Newton iterations are considered converged if either the Newton step size is less than $\varepsilon = 10^{-5}$, or 10 iterations have been made. The 10 iterations can be seen as a large upper bound on the number of iterations that this problem should require before converging. If more than 10 Newton iterations are required to solve a single step of the solution process, then something is wrong with the convergence of the numeric algorithm.

Contact methods

The dynamic problem (2.11) with the same boundary conditions as given in (6.10) and initial conditions given by

$$y_0(x) = y_{\text{ref}}(x) \qquad v_0(x) = 0 \qquad (6.11)$$

is solved using the three contact methods. They are compared in terms of usability (how good solutions are found), performance (are many Newton steps required per time step) and stability (does the Newton method converge each time step).

The idea behind these boundary and initial conditions is as follows. The initial condition is the reference solution, i.e. the analytical solution of the static problem with $y(t, 0) = 1$ and $y'(t, 0) = -1/2$. If the contact method were perfect, the dynamic solution would be equal to the reference solution for all t , and the solution would be stable. However, the contact methods are not perfect so the solution will violate the contact constraint in some places. The solutions will then show some dynamics which can be compared.

Explanation for interpretation of the plots: In the following paragraphs, figures are going to be referenced which contain the same kind of plots for all simulations of the dynamic problem. The leftmost plot is the solution $y(t, x)$, where $x = 0$ is on the left side and $x = L$ is on the bottom. Over time, the beam's position moves as if a slice is taken perpendicular to the time axis. The middle plot is the value of λ , where the x and t directions are positioned in the same manner. Finally a Newton iteration plot is given. For each time step (of length τ), some number of Newton iterations are made. For each iteration, the Newton step size is shown as a \bullet . Furthermore, for each time step the total number of Newton iterations is indicated with a label at the last \bullet . If this number is large or the \bullet 's are close together, there is bad convergence. It is not possible to see where λ is updated in this plot.

Penalty method For both $p = 10^2$ and $p = 10^4$ the results of the simulation are shown in fig. 6.6. For a lower value of p there is significant penetration of the surface, where the solution 'bounces' up and down. Once the

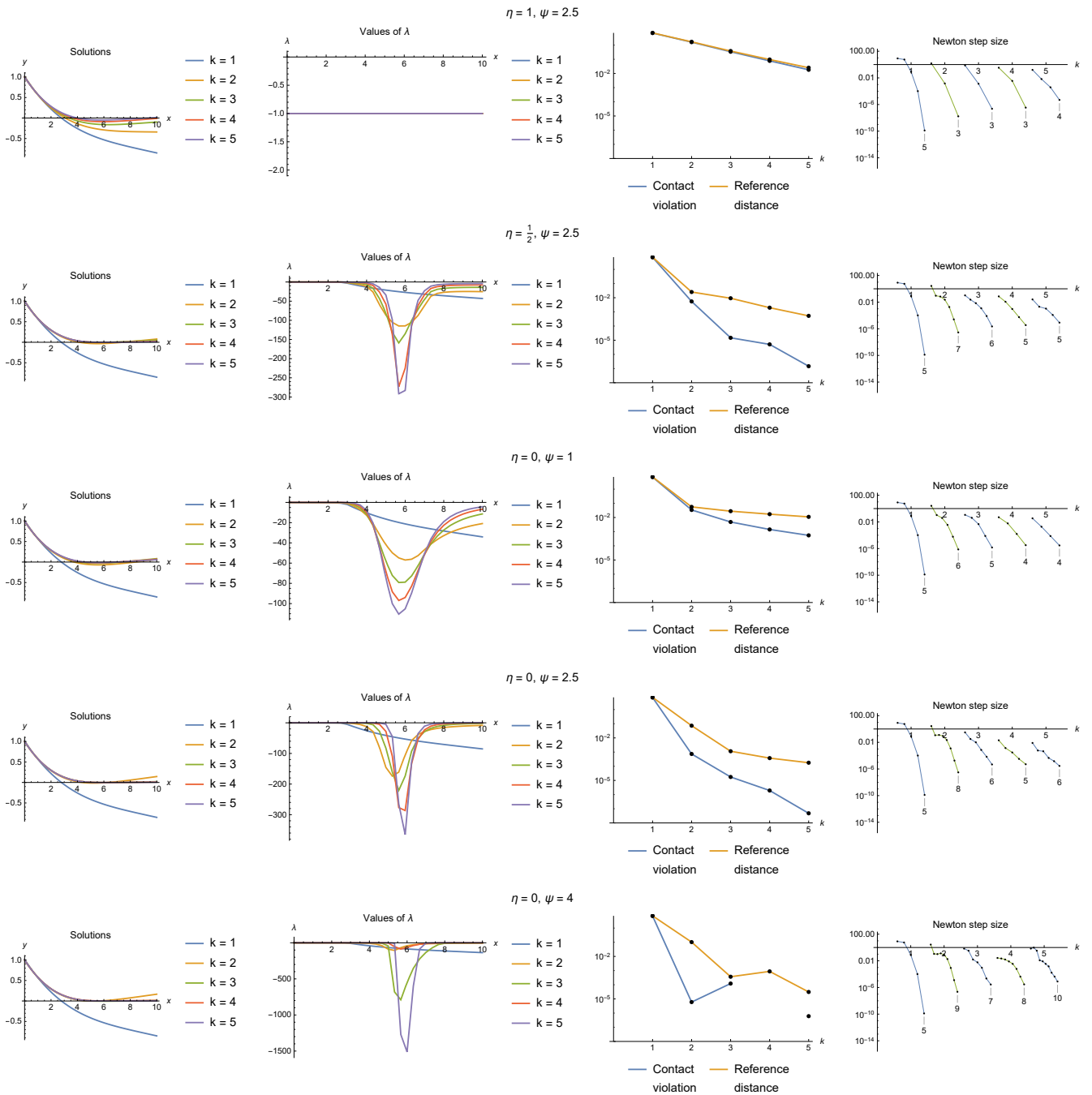


FIGURE 6.5: The solution of the static problem with the value of λ , a convergence plot and the Newton step sizes, using $\eta \in \{0, 1/2, 1\}$, $p_0 = 10^2$ and $\psi \in \{1, 2.5, 4\}$.

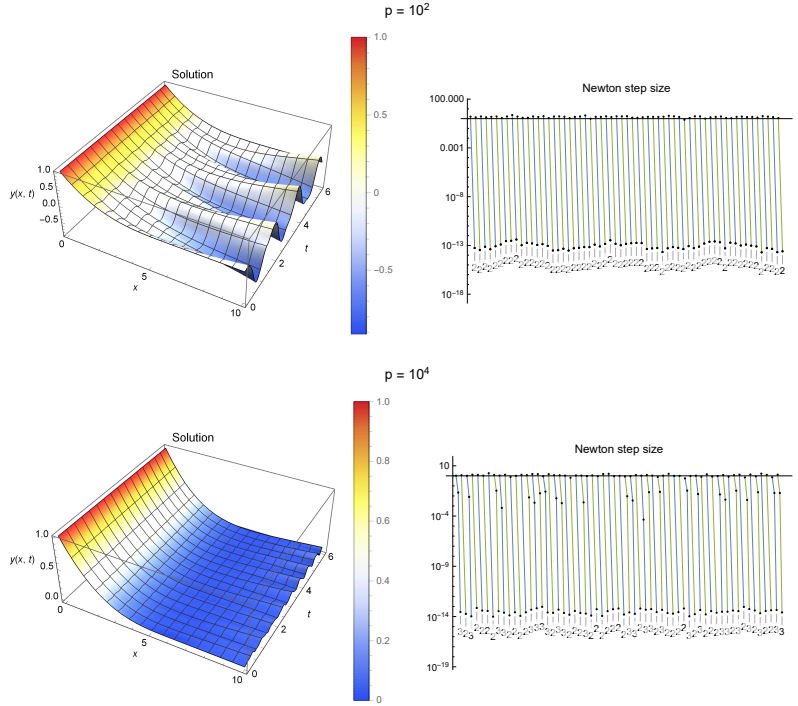


FIGURE 6.6: Two solutions of the dynamic problem with contact enforced by the Penalty method, for $p = 10^2$ and $p = 10^4$.

value of p is increased, the ‘bouncing’ still occurs, but is reduced a lot. The solution is very close to the initial condition y_{ref} , just like it should be. The Newton convergence is very good: for both values of p at most 3 Newton steps are required per time step.

Augmented Lagrangian method The Augmented Lagrangian method has been tested on the dynamic problem for both updating schemes for λ and p , and for two instances of the penalty parameter ($p = 10^2$ and $p = 10^4$).

For *Scheme 1* the results can be found in fig. 6.7 During contact and during the solution process bad Newton convergence can be observed because more than 10 Newton steps are required per time step. This makes the solution unusable because many of the time integration steps have not converged.

For *Scheme 2* the results can be found in fig. 6.8. In this situation better results can be observed. The Newton convergence is better (although some time steps have not converged for higher values of p). It can be seen that the solution does not seem realistic: it is ‘shot’ away from its equilibrium by the contact method which adds energy to the solution on each contact. Considering it this way, the Lagrangian parameter works too well for enforcing contact and energy in the system is not conserved.

Augmented Barrier method In fig. 6.9 the results for the dynamic problem with the Augmented Barrier method can be seen for penalty parameter values $p = 10^{-1}$ and $p = 10$, and using *Scheme 2* for updating the λ and p values. It can be seen clearly that once contact is initiated, the value of λ rises (in absolute value) quicker than when using the Augmented Lagrangian method. Because of this value, a large ‘push’ is given to the solution which ‘shoots’ away. In comparison to the Augmented Lagrangian method, the Newton convergence is better: there are no time integration steps where the limit of 10 Newton steps is reached. Even then, the solutions are unrealistic and not practically usable.

Numerical damping

Using the Penalty method to enforce contact, the dynamic problem (2.11) with boundary conditions

$$y(t, 0) = 1 + \frac{1}{4} \sin\left(\frac{3}{10}t\right), \quad y'(t, 0) = -\frac{1}{2}, \quad EIy''(t, L) = 0, \quad EIy'''(t, L) = 0, \quad (6.12)$$

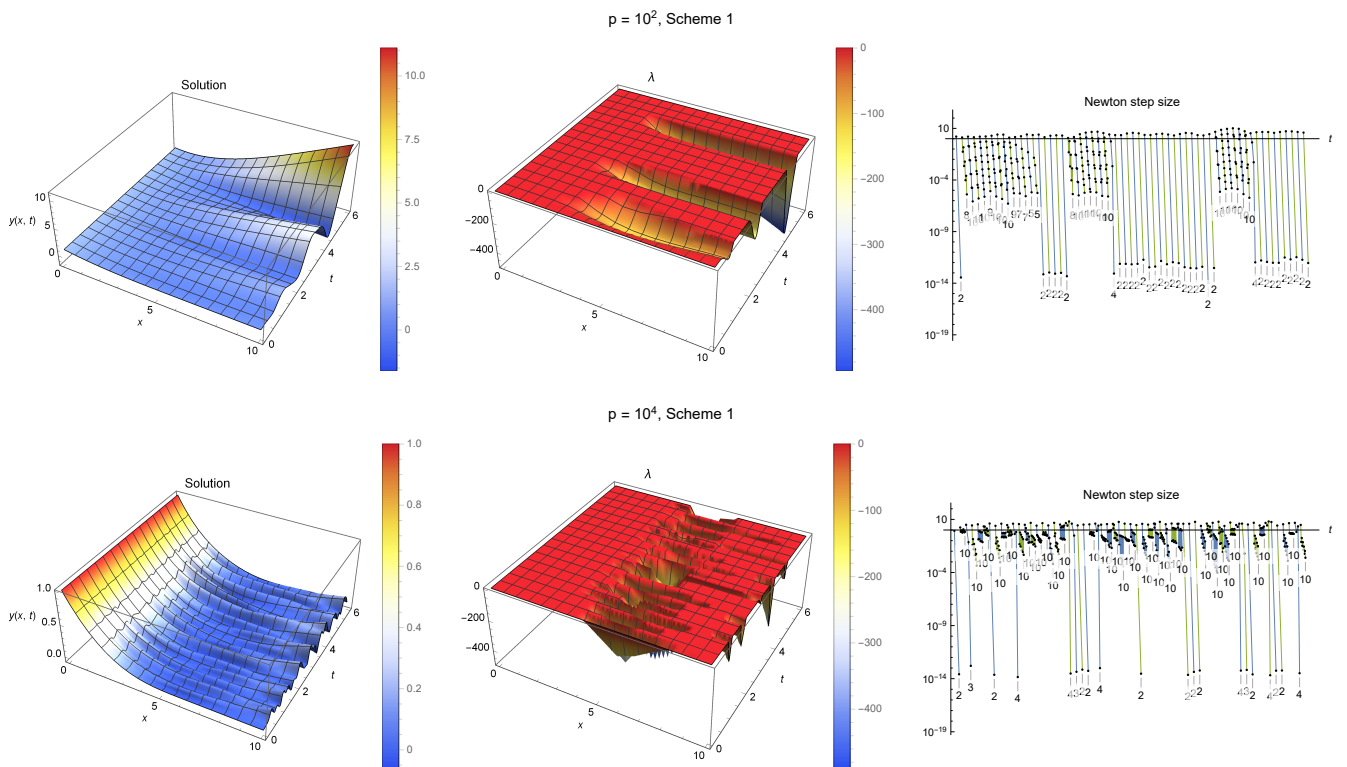


FIGURE 6.7: Augmented Lagrangian method solution for the dynamic problem using *Scheme 1* for $p = 10^2$ and $p = 10^4$.

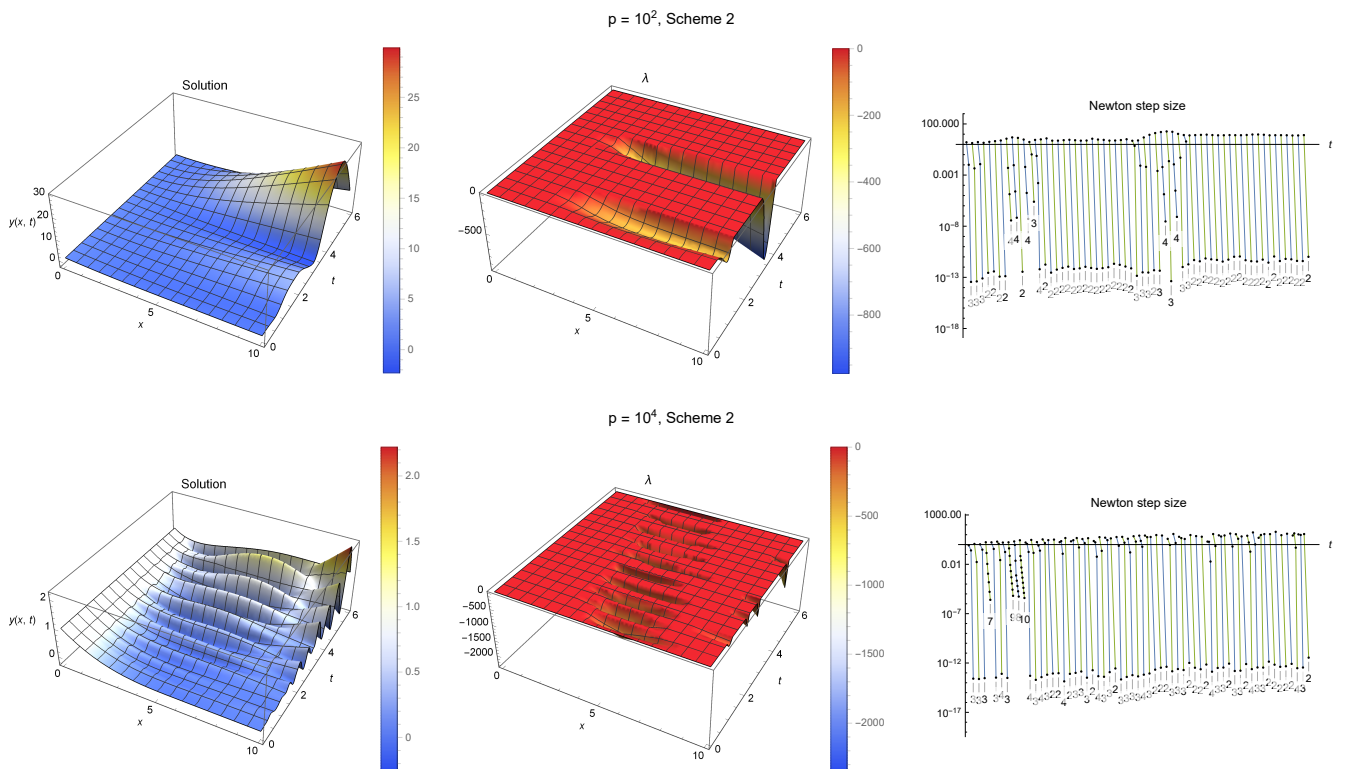


FIGURE 6.8: Augmented Lagrangian method solution for the dynamic problem, using *Scheme 2* for $p = 10^2$ and $p = 10^4$.

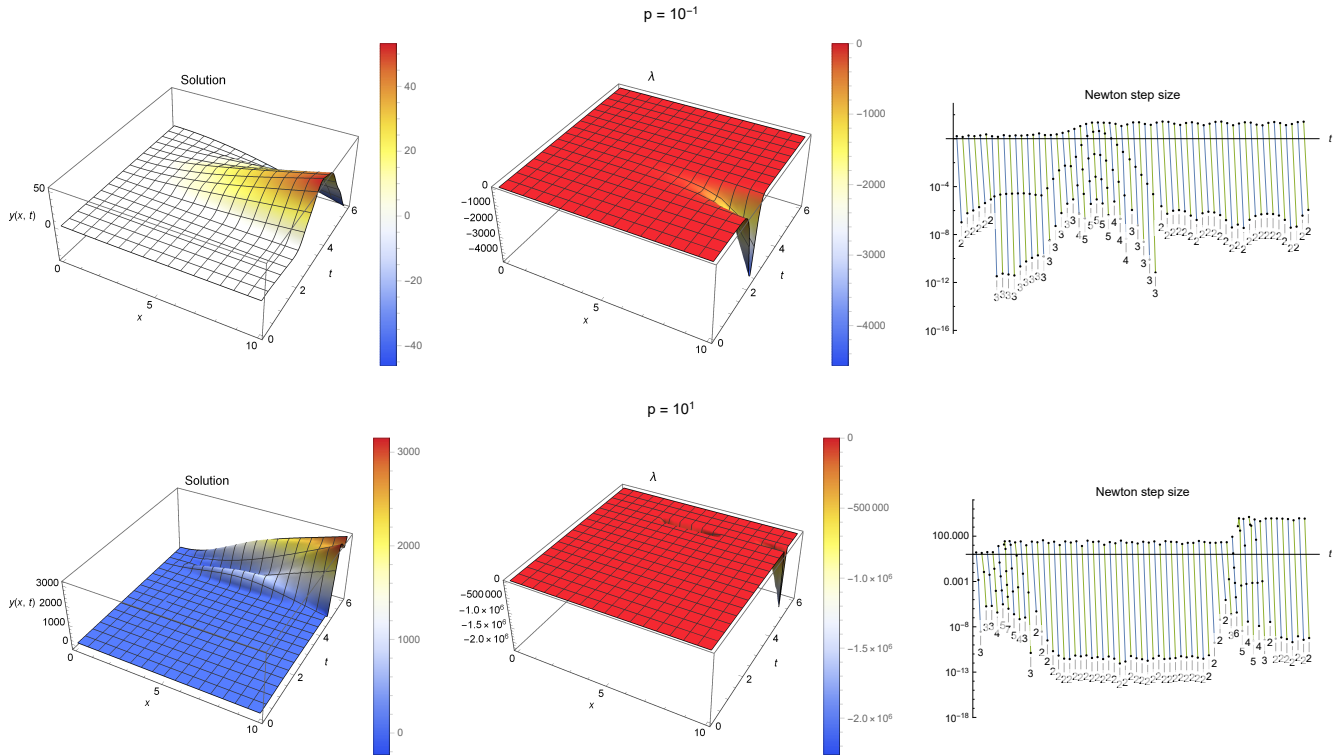


FIGURE 6.9: Augmented Barrier method solution for the dynamic problem, using *Scheme 2* for $p = 10^{-1}$ and $p = 10$.

is solved for a long time ($t \in [0, 15]$) with (large) time steps of $\tau = 0.2$ [s/step]. The penalty parameter is $p = 10^4$ and $N = 20$ elements are used. The material constants are $EI = 10^4$ [Nm²], $\mu = 10$ [N/m] and $L = 10$ [m]. The value of α is varied, to show the increase in time integration stability for $\alpha > 0$. Figure 6.10 shows the results. We can see that a value of $\alpha = 0.05$ decreases the high-frequency oscillations of the end of the beam at $x = L$ that are numerical errors caused by contact with the surface.

The largest time steps which can be used for a certain value of α depend on the contact surface, the problem parameters and the convergence of the Newton method in these situations.

Comparison of contact methods

This section describes a short comparison on the different contact methods. After comparing the three methods for solving the dynamic problem, it seems that only the Penalty method gives a good solution, and both Augmented methods seem to ‘shoot’ away the solution. This causes solutions which are not representing the expected solution and show bad Newton convergence.

The Augmented Lagrangian and Augmented Barrier methods both shoot the solution away, equivalent to giving the beam a lot of energy in a short timespan while in contact with the surface. Before concluding that the Augmented contact methods are no use because of this problem, a specific and easier dynamic problem is investigated which gives more information about the behaviour of the contact methods.

We analyze the behaviour of the three contact methods on the problem of a bouncing ball under influence of gravity. The well known model for the height of the ball $y(t)$ [m] is given by

$$m\ddot{y}(t) = -mg \quad y(0) = y_0, \quad \dot{y}(0) = v_0, \quad (6.13)$$

with m [kg] the mass of the ball and g [m/s²] the gravitational constant. The solution is a simple parabolic trajectory, with its coefficients depending on the initial conditions y_0 [m] and v_0 [m/s].

We enforce contact (the constraint $y(t) \geq 0$) by introducing the penalty function $\Xi(d_N(y))$ with a penalty parameter p , depending on the used contact method (Penalty, Augmented Lagrangian or Augmented Barrier). This

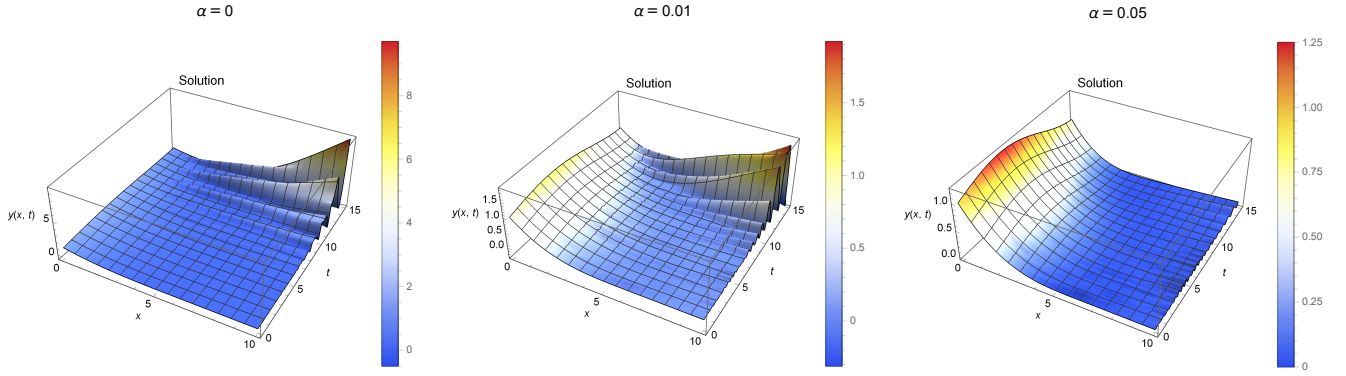


FIGURE 6.10: Solution with contact enforced by the Penalty method ($p = 10^4$) running for $T = 15$ seconds, with time step $\tau = 0.2$. The value of α is varied between 0 and 0.05.

gives the new (non-linear) form of (6.13) as

$$m\ddot{y}(t) + \Xi(d_N(y(t))) = -mg, \quad y(0) = y_0, \quad \dot{y}(0) = v_0. \quad (6.14)$$

For this comparison, a normal Euler-forward (explicit) integration scheme has been implemented. The usual tools in MATHEMATICA and MATLAB do not support solving of differential equations with an update rule (required for the value of λ in the latter two contact methods) each time step. However, this simple implementation already shows the sought effects.

Figure 6.11 shows the results of the implementation and simulation, using the initial values $y_0 = 10$ [m] and $v_0 = 0$ [m/s]. A timespan of 5 seconds ($T = 5$ [s]) is simulated with high precision ($\tau = 0.001$ [s/step]) to see the effect of once single bounce of the ball, and $m = 1$ [kg] and $g = 10$ [m/s²] are chosen. The contact methods enforce the constraint $y(t) \geq 0$ using their penalty function $\Xi(d_N(y))$. Note that the Penalty method does use any value of λ , so that visualisation is not shown. The potential $U(t)$ and kinetic energy $K(t)$ are respectively given by

$$U(t) = mgy(t), \quad K(t) = \frac{1}{2}m\dot{y}(t)^2. \quad (6.15)$$

We observe some features in the solution when comparing the three methods. All the three methods make the ball bounce on the ground. The Augmented Lagrangian shows less violation of the solution constraint in comparison to the Penalty method, and the Augmented Barrier method shows less violation of the solution constraint in comparison to the Augmented Lagrangian method, even though the values of p are equal or lower for the latter two methods. Note that the value of p should not influence the energy levels in the system, only the precision of the contact enforcement (which may require smaller integration time steps).

For the Penalty method, the total energy levels stay equal after a bounce (up to numerical errors due to simple integration scheme). For the latter two methods, the energy levels show a huge increase after the bounce, where the Augmented Barrier is much more explosive compared to the Augmented Lagrangian method. Although it is not displayed, increasing the value of p makes all three contact methods more aggressive: there is less contact violation.

Using these observations, a (general) conclusion about the contact methods for dynamic problems can be formulated. The Penalty method is the only suitable method for enforcing contact for a one-dimensional object. The latter two methods are *too good*: they enforce contact so well that too much energy is added to the system, resulting in non-realistic (and undesired) behaviour which yields no usable solutions.

This conclusion is also partially representative for the dynamic beam model, because it is also single dimensional, although elements are connected to each other, partially slowing down a single element and absorbing some of its generated energy. We refer also to Section 7.2 for a recommendation on possible ways to solve these problems.

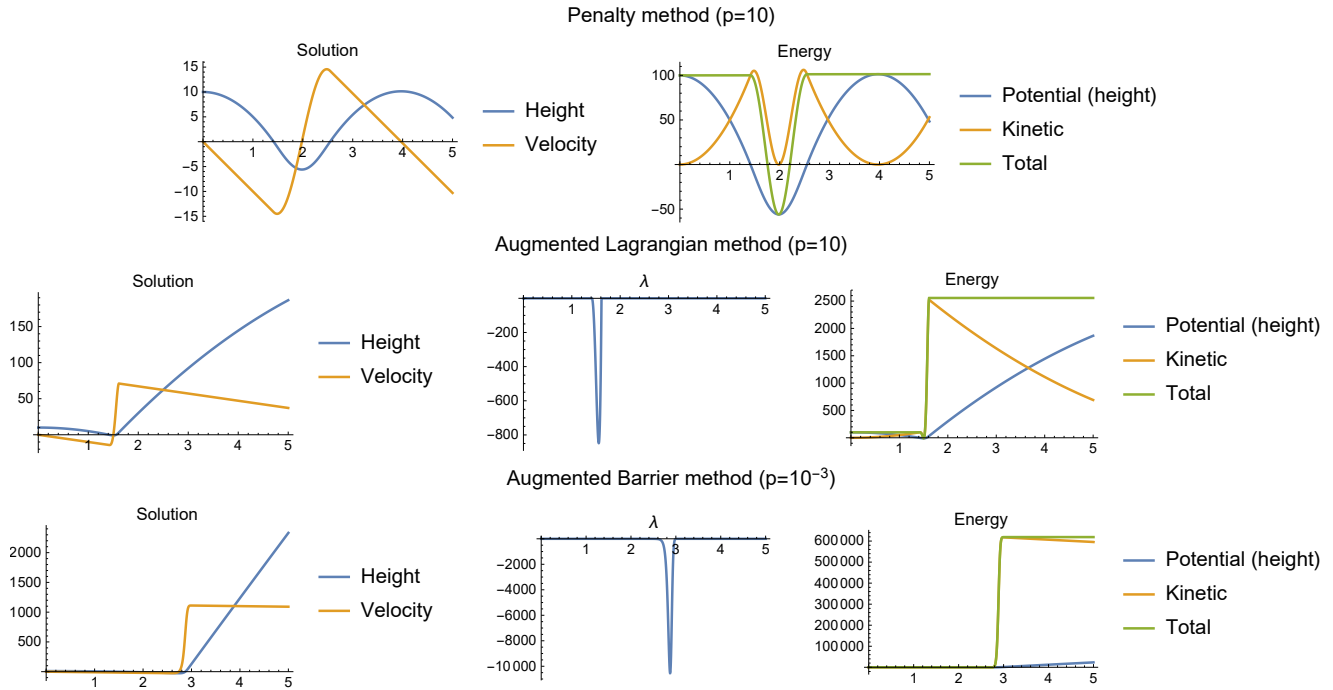


FIGURE 6.11: Visualizations of simulations comparing the bouncing ball using three contact methods. The solutions show the height and velocity of the ball, the value of λ (if applicable) and the energy levels in the system (potential and kinetic).

6.3 Integration interpolation

In section Section 4.1.4 Gauss-Legendre interpolation is introduced in favour of the Trapezium rule for approximation of integrals. In this section a comparison is made between the two method of approximation.

The static problem (2.13) is solved with the boundary conditions (6.10). The used contact method is the Augmented Barrier method with $p_0 = 10$ and $\psi = 2.5$. The used parameters are $EI = 10^4$ [Nm²], $\mu = 10$ [kg/m], $L = 10$ [m] and $N = 5$ elements have been used. The low number of elements are chosen such that it is possible to see the influence of the integration approximation on the precision and convergence of the solution.

In figure 6.12 the results of the comparison are given. It is clear that there is only a small difference in terms of contact violation, although the Gauss-Legendre interpolation seems to converge more steadily towards small errors. The Newton convergence is very similar between the two methods. The only thing which stands out is the way the solutions look. For the trapezium interpolation there is more penetration in the middle section and the deflection is higher in the right section of the pipe. For the Gauss-Legendre interpolation the solution is flatter as lies on the contact surface.

This comparison has also been done for the other contact methods. The results are similar to the results found for the Augmented Barrier method.

6.4 Damping

The two different kinds of damping are compared in this section. For each of the damping types, a different problem is used because the goals of the damping are different. Structural damping is meant for damping the entire solution, while damping on contact only dissipates energy on contact.

6.4.1 Structural damping

In fig. 6.13 a comparison is given between a damped and an undamped solution of the problem (2.11) without distributed load or contact and homogeneous boundary conditions

$$y(t, 0) = 0, \quad y'(t, 0) = 0 \quad EIy''(t, L) = 0, \quad EIy'''(t, L) = 0, \quad (6.16)$$

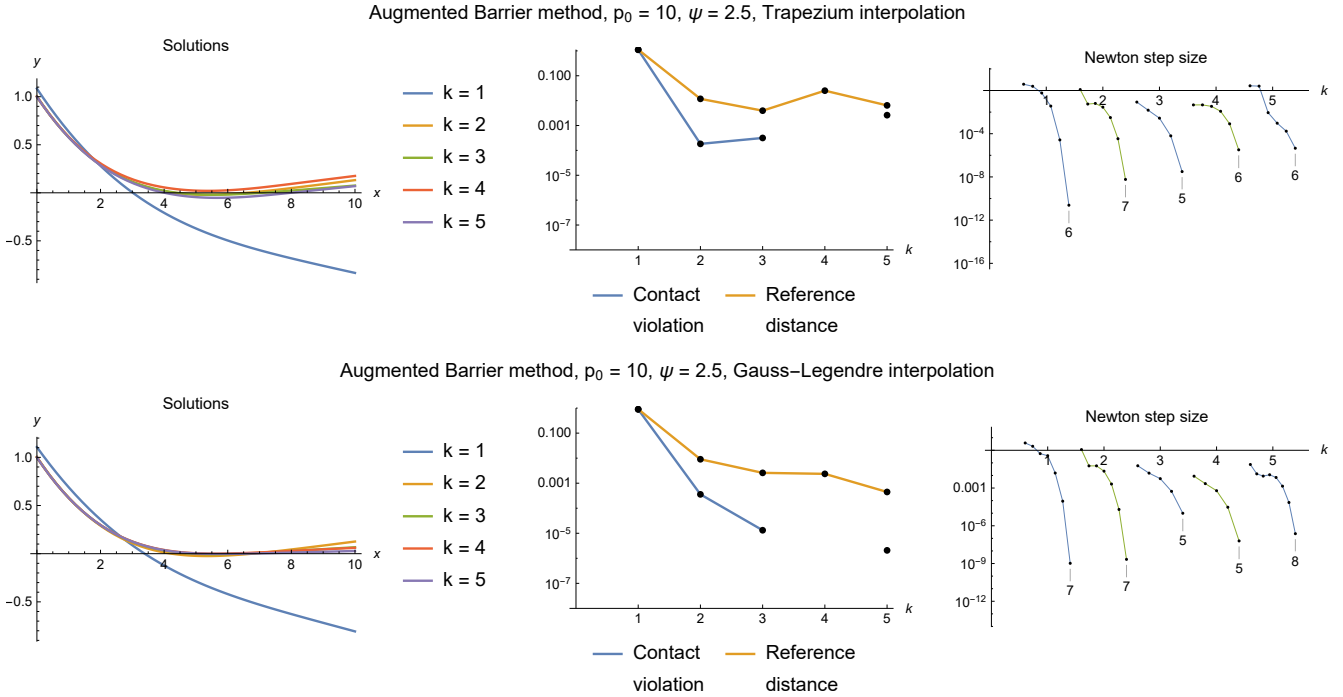


FIGURE 6.12: A comparison of the two integration methods: Trapezium and Gauss-Legendre interpolation.

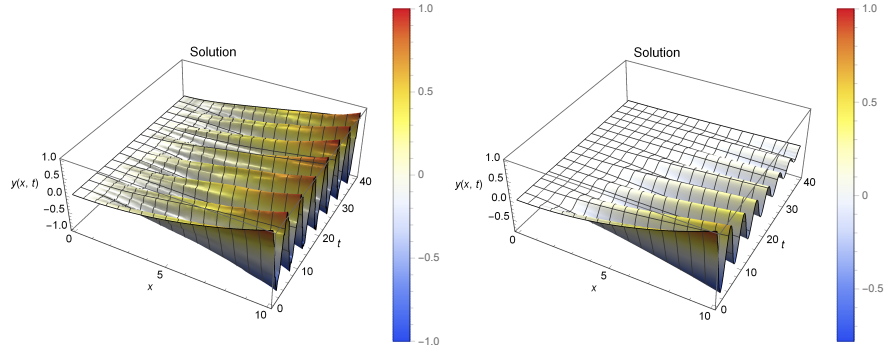


FIGURE 6.13: A comparison of a vibrating beam with no contact with ($\alpha_1 = \alpha_2 = 0$) and without ($\alpha_1 = \alpha_2 = 0.05$) structural damping.

and initial conditions $y_0(x) = (x/L)^2$ and $v_0(x) = 0$. The used parameters are $EI = 10^4$ [Nm²], $\mu = 10$ [kg/m] and $L = 10$ [m], and take $T = 5$ [s], $\tau = 0.1$ [s/step] and $\alpha = 0$. For $\alpha_1 = \alpha_2 = 0$ no damping occurs and the solution is a sinusoid in the temporal direction. For the parameters $\alpha_1 = \alpha_2 = 0.05$ which make the C matrix (see Section 4.1.3) non-zero, damping occurs and energy of the beam is dissipated.

6.4.2 Damping on contact

In order to test and analyze the damping on contact with the contact surface as determined in Section 3.5, the boundary conditions are chosen as

$$y(t, 0) = 1, \quad y'(t, 0) = -\frac{1}{2} + \frac{1}{2}e^{-t} \quad EIy''(t, L) = 0, \quad EIy'''(t, L) = 0, \quad (6.17)$$

and the initial conditions as $y_0(x) = 1$, $v_0(x) = 0$. These boundary and initial conditions simulate the beam ‘slamming’ into the ground by twisting the beam at $x = 0$ until the boundary conditions are conform the reference solution y_{ref} . The expected dynamic solution is a bouncing pipe on the seabed, until the damping force during contact will stop the pipe’s movements.

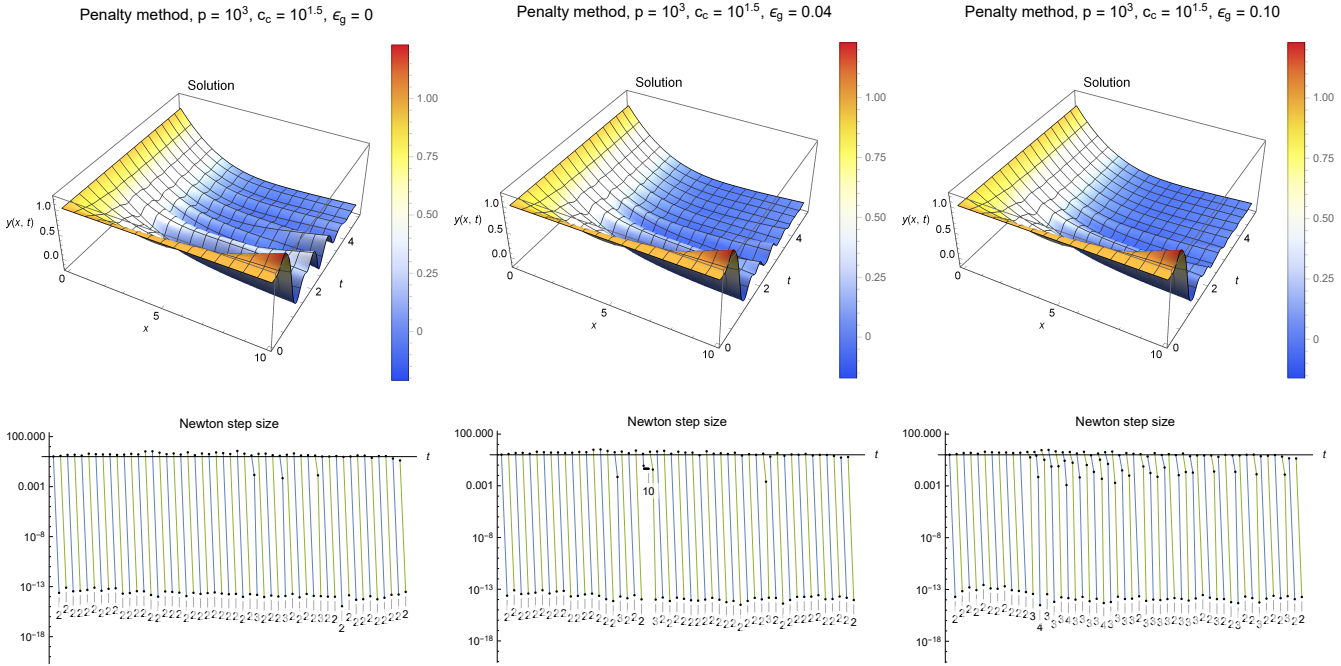


FIGURE 6.14: Damped solution for the Penalty method with $p = 10^4$, $c_c = 10^{1.5}$ and $\varepsilon_g \in [0, 0.1]$.

Furthermore, we use the parameters $EI = 10^4$ [Nm²], $\mu = 10$ [kg/m] and $L = 10$ [m], and take $T = 5$ [s], $\tau = 0.1$ [s/step] and $\alpha = 0$. A good value for c_c seems to be \sqrt{p} , where p is the penalty parameter of the contact method. This observation is open for further investigation because the value of p influences the time spent below the contact surface considerably and fine-tuning may be required to get the required results.

Only the Penalty method has been used here for damping on contact because of the reasons mentioned in Section 6.2.2. For completeness solutions using the other two contact methods are shown in Appendix A.4. An undamped, lightly damped and over-damped solution is shown using $p = 10^3$ and $c_c = 10^{1.5}$ in fig. 6.14, while varying the parameter ε_g in the interval $[0, 0.1]$.

The solution behaves as expected, where the solution damps out much quicker if the value of ε_g is increased. The solution also dampens quicker if the value of the damping parameter c_c is increased (not shown in figures). It is not sensible to determine a damping constant for these solutions in order to compare the damping properties of the solution in the long term. After all, the solution may be damped a lot during contact but make very little contact, or it may make a lot of contact but be damped very little during contact, resulting in the same damping properties but very different solutions.

Finally it can be noticed that during a single time step bad Newton convergence can occur (for example about halfway in the convergence plot for the problem with $\varepsilon_g = 0.04$ in figure fig. 6.14), although it does not seem to affect the rest of the solution.

Other values of c_c are not shown here because the solution will either be over-damped or under-damped which does not give insightful solutions.

6.5 Shape of contact surface

This section described different shapes of contact surfaces. The seabed is usually relatively flat but can also contain bumps or ridges. Furthermore, the stinger which supports the beam as it is lowered into the sea consists of rollers which make contact with the pipe, while the rest of the beam is free.

In the previous sections the contact surface given by $f(x) = 0$ has been used as the contact constraint. In order to demonstrate the applicability of the contact methods on other surfaces two problems have been solved.

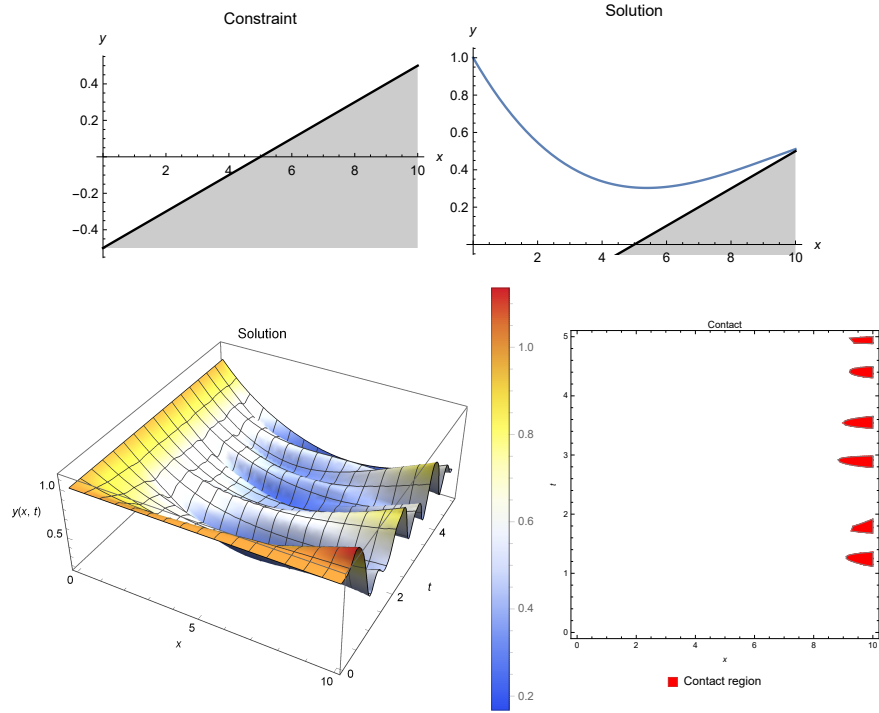


FIGURE 6.15: Problem with constraint $d_N(y) = y^{-1/10}(x - L/2) \geq 0$. The constraint and static solution are shown above and the dynamic solution with the associated contact region is shown below.

The first problem is given by (2.11) (no damping or distributed load) with

$$y(t, 0) = 1 \quad y'(t, 0) = \frac{3}{10} (e^{-t} - 1) \quad EIy''(t, L) = 0 \quad EIy'''(t, L) = 0 \quad (6.18)$$

and initial conditions $y_0(x) = 1$, $v_0(x) = 0$. The solution constraint $y \geq 1/10(x - L/2)$ (and $d_N(y) = y^{-1/10}(x - L/2)$) is used which can be seen as a flat but tilted surface. The usual parameters $EI = 10^4$ [Nm²], $\mu = 10$ [kg/m], $L = 10$ [m], $\tau = 0.1$ [s], $\alpha = 0$, $T = 5$ [s] and $N = 10$ elements are used. The contact is enforced using the Penalty method with $p = 10^4$. The constraint and the result (dynamic and static solutions) are given in fig. 6.15. For the static solution the time limit of the boundary is taken, $y'(0) = -3/10$. The right side of the solution can be seen to stay well positive, while the middle side is allowed to vibrate more violently.

The second problem is given by (2.11) (no damping or distributed load) with

$$y(t, 0) = 1 - \sin(t) \quad y'(t, 0) = 0 \quad EIy''(t, L) = 0 \quad EIy'''(t, L) = 0 \quad (6.19)$$

and initial conditions $y_0(x) = 1$ and $v_0(x) = 0$. The solution constraint is given by $y \geq 1 - (x - L/2)^2$ (and $d_N(y) = y - (x - L/2)^2$) which can be seen as a single bump in the contact surface which the solution may not penetrate. This is the case for a single roller on the stinger which supports the pipe. The parameters and contact method are the same as for the first problem, and the result (dynamic and static solutions) is shown in fig. 6.16. For the static solution the boundary has no limit so a single value is taken, $y'(0) = -1/2$. The solution is ‘wobbling’ over the point $x = L/2$ where contact is enforced.

6.6 Simplification for point of contact

Often the location of the pipe where contact is initiated is of specific interest. The movements of the pipe make the point of contact move. Too large movements cause problems and may damage the pipe. In those situations the exact dynamics and movements of the pipe are of less interest. In this section we explore a way to approximate

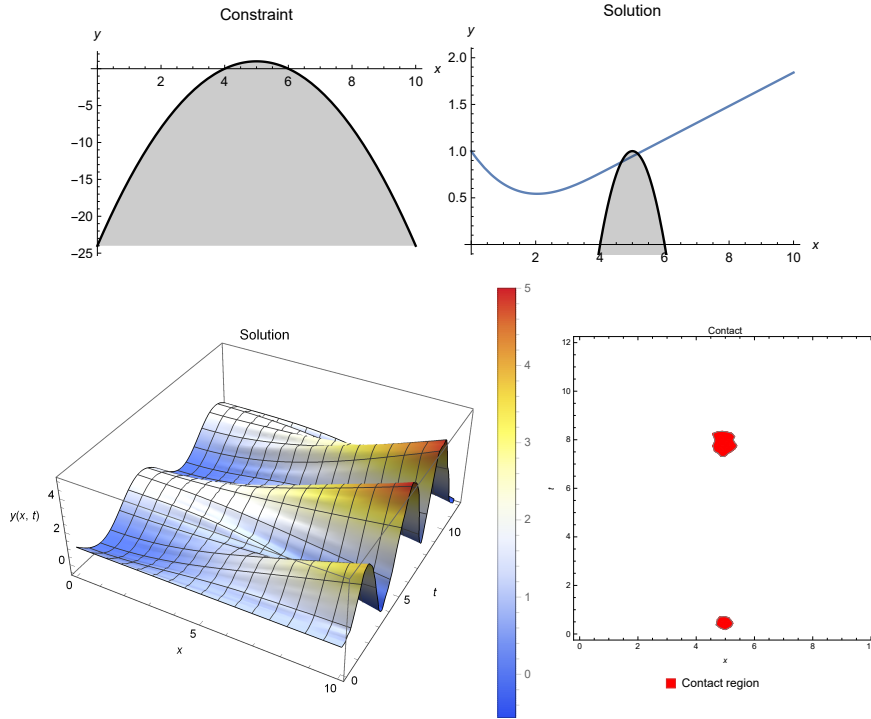


FIGURE 6.16: Problem with constraint $d_N(y) = y - (1 - (x - L/2)^2) \geq 0$. The constraint and static solution are shown above and the dynamic solution with the associated contact region is shown below.

the location of contact by using the (analytical) static solution without requiring the calculation of the dynamic problem solution. This result is motivated by some simulation examples with dynamic boundary conditions.

In order to analyze this specific scenario where only the point of contact is requested and not the entire solution of the pipe, a simplification is proposed for the solution method. The problem where the pipe's location and angle is known on one side ($x = 0$), and free on the other side is considered ($x = L$). The parameters and boundary conditions are chosen such that that the point of contact is guaranteed to be in between the start and end point of the beam. Concretely, we solve (2.11) with no damping ($c_d = 0$), and with the boundary conditions

$$y(t, 0) \quad y'(t, 0) \quad EIy''(t, L) = 0 \quad EIy'''(t, L) = 0 \quad (6.20)$$

where $y(t, 0)$ and $y'(t, 0)$ will be specified along with the initial conditions.

Point of contact We are interested in the first point of contact x_C at each time t , given by the expression

$$x_C(t) = \min \left\{ x \in [0, L] \mid y(t, x) \leq 0 \right\} \quad (6.21)$$

Notice two things. First of all $x_C(t)$ may be undefined if there is no point of contact in the domain (the pipe is flying loose from the ground). Hopefully this does not happen in practice, although it may definitely occur during the process of finding a numerical solution. Furthermore, the description here is a minimization problem in terms of the solution, which requires the solution at some time t to be known. This might be solved by approximating $x_C(t)$ based on $x_C(t - \tau)$ for some small value of τ .

Using the solution of the dynamic problem in order to calculate the point of contact is abandoned in favour of the following approximation which does not require the dynamic problem solution.

Approximation The point $x_C(t)$ or a good approximation thereof can be solved in a different way. We approximate the dynamic solution at point in time with the static solution using the boundary conditions at that point in time.

In some situations the static solution can be calculated analytically. See Section 4.2 where the reference solution $y_{\text{ref}}(x)$ is calculated as a solution of the static problem, given $y(t, 0) > 0$ and $y'(t, 0) < 0$. For an analytical solution to the static problem, the extra parameter is the point of contact \hat{L} which is solved along with the static solution as an extra parameter. If the dynamics of the pipe do not influence the contact point a lot, the contact point x_C of the dynamic solution may be approximated by the contact point $\hat{L} = -3(y(t, 0)/y'(t, 0))$ of the static solution (in short: $x_C \approx \hat{L}$).

This approximation has been tested for various (time-dependent) boundary conditions. Both the solution to the dynamic problem and the approximation of the point of contact have been calculated. The results can be found in fig. 6.17. The red region describes the contact region ($y(t, x) \leq 0$) and has been determined numerically from the dynamic solution. The blue line denotes the approximation $x_C \approx \hat{L}$ using the method above and only uses the analytic static solution for the given boundary conditions. For all problem instances, the parameters $EI = 10^4$ [Nm⁻²], $\mu = 10$ [kg/m], $N = 25$ elements, $T = 6$ [s], $\tau = 0.1$ [s/step], $\alpha = 0.05$ (to remove high-frequency contact oscillations) and $L = 10$ [m] have been used. The boundary conditions vary, from a changing position $y(t, 0)$ to changing angle $y'(t, 0)$ or a combination. To model the contact, the Penalty method has been used with $p = 10^4$ and without any damping or distributed load.

Observations Some things can be concluded from fig. 6.17. The approximation using the static solution does *not* describe the left boundary of the region of contact but rather the centre. This is a good thing: because of the contact modelling method, some penetration must occur. For a perfect contact solution, the solution would be locally ‘lifted up’ around the location x_C where contact is initiated resulting in the very small contact region indicated by the approximation. Also the boundary of the contact region fluctuates much, more than the actual point of contact moves over the contact surface. For this reason it is not advisable to even consider using the actual numerical value of x_C which could be determined from a numerical solution.

Furthermore, even for quite large oscillations, the approximations seems to follow the contact region well. Only in the last problem instance (bottom right plots in fig. 6.17) where the solution is ‘dropped down’ onto the seabed, the values of $y(t, 0)$ and $y'(t, 0)$ both approach zero. This makes the contact region and the approximation both less accurate. This is logical since the static contact point is given by $-3(y(t, 0)/y'(t, 0))$ and if $y'(t, 0)$ approaches 0 the numerical errors grow ever larger.

Finally, this approximation only works when $y'(t, 0) < 0$. This means that in case of such a large deflection of the beam such that $y'(t, 0) > 0$, the approximation is not defined. However, this situation does not seem a realistic scenario occurring with an actual pipe.

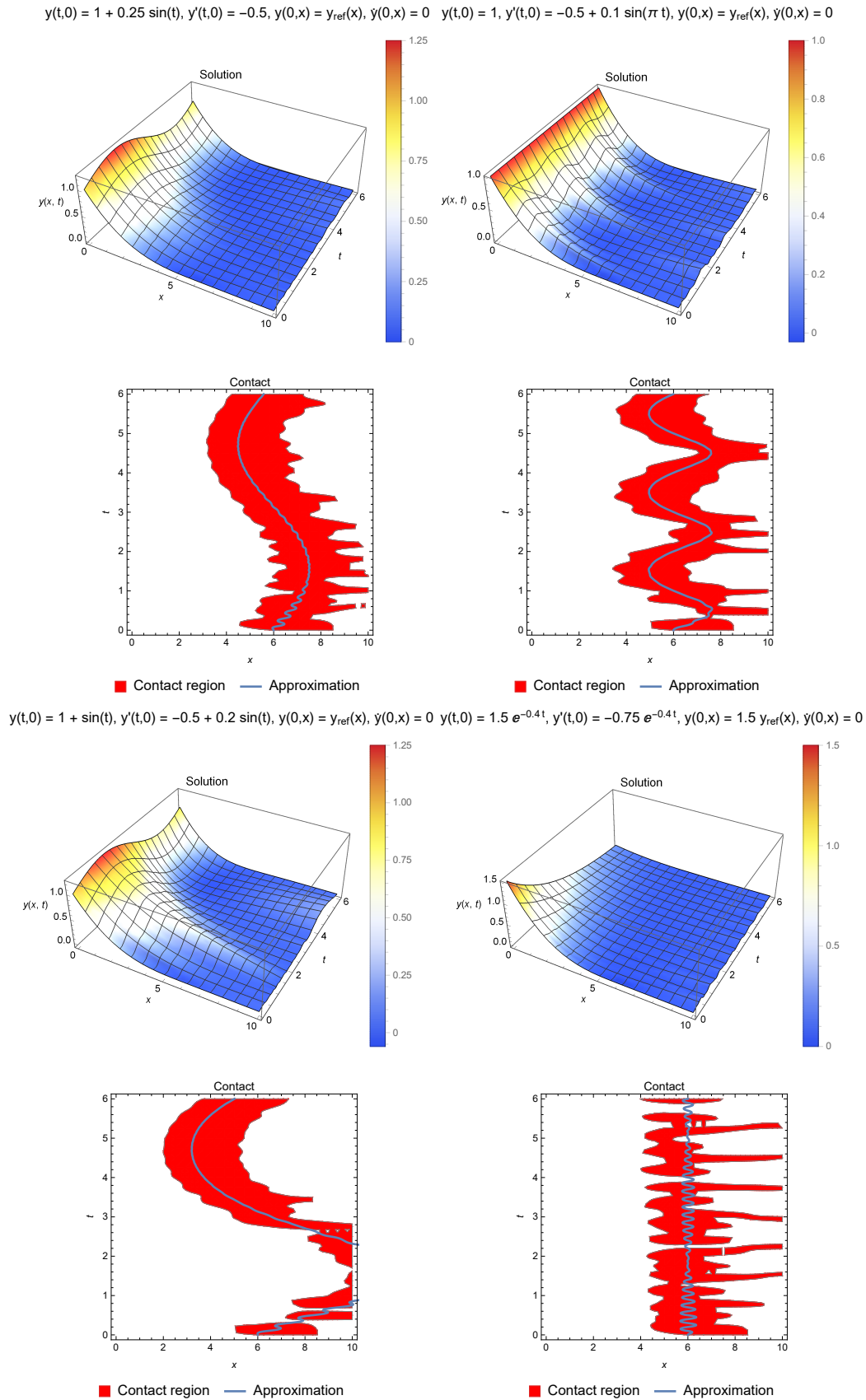


FIGURE 6.17: Contact region determined by the dynamic solution (red region) and the approximation of the contact point (blue line) using the analytic static solution, for multiple instances with different boundary and initial conditions. It can be seen that the centre of the contact region is approximated well by the static solution contact approximation.

Chapter 7

Conclusion & recommendations

In this thesis solution methods have been explored for the pipelaying problem. A mathematical model has been made for three sections of the pipe, which allows implementing the three presented contact methods. To solve the problems numerically, a Finite Element derivation and implementation has been made and verified against analytical results. The three contact methods have been compared for precision, convergence and numerical stability.

For the static problem, the equilibrium of the pipe, all three methods work well and give sufficient results. By using the more advanced methods (Augmented Lagrangian and Augmented Barrier method), a better stability and convergence rate can be achieved. For the dynamical problem, the movements and dynamics of the pipe, only the Penalty method works as expected: contact is enforced and the solutions show preservation of energy in the system. The other two contact methods solve the problem but add too much energy to the dynamical system giving nonsensical results. Concretely, the Penalty method should be used for solving dynamical problems.

In addition to the contact methods, attempts have been made to simplify the solution process. First of all the middle section of the pipe (without contact) can be represented via a transfer function which removes the need to solve the entire problem. Secondly, the point of contact with the seabed can be represented by the point of contact of a static solution which makes finding the required solutions more efficient.

7.1 Application overview

A possible way to apply the Finite Element derivations as well as the simplifications is as follows. Assuming the ships movements are known, a full Finite Element simulation including contact can be performed of the part of the pipe which may make contact with the stinger (section I in fig. 2.1). The right side of the pipe has known deflection and angle boundary conditions. The left side which is suspended into the water has a force and torque boundary condition due to the missing rest of the pipe for this section.

The approximation of the transfer function can be used for the middle section of the pipe (section II in fig. 2.1). The deflection and angle of the upper part of the pipe can be found from the simulation of the first pipe section. The bottom boundary conditions can be seen as a free end with some force and torque working on that end, depending on the weight of the pipe. By transforming the numerical boundary condition data into the Laplace domain, the deflection and angle of the lower part can be found and/or approximated with the process outlined in Chapter 5.

Finally the section resting partially on the seabed (section III in fig. 2.1) can be approximated by the static solution in many occasions in order to find the point of contact. Depending on the nature of the deflection and angle found as a solution of the middle section of the pipe, the static solution may be valid or not. If it is, the position of the pipe and the place of contact with the seabed can be calculated efficiently. In case the static solution is not valid, the dynamic Finite Element solution must also be calculated for the part of the beam lying on the seabed. The left side, where the end of the pipe is connected to the already laid pipe on the seabed, can be considered as a fixed and static deflection and angle.

Special care must be taken because of the up and down movements of the ship because this moves the reference frame for the simulation and approximations. Also, in case large deflections occur the model presented in

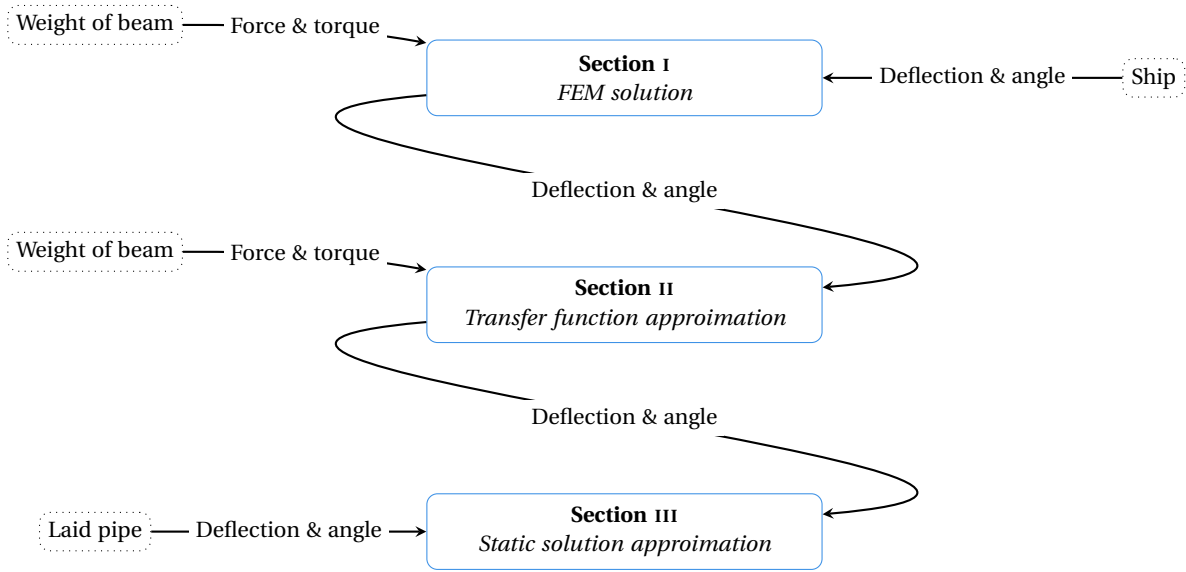


FIGURE 7.1: A schematic overview of the application of the Finite Element derivations and simplifications. Arrows towards a section denote the known boundary conditions for that side of the problem. Arrows pointing outwards denote the parts of the solution for that section that are required for the next section.

Chapter 2 is not valid and must be replaced with another Finite Element model such as the co-rotational method. Finally, because the force and torques must be known in order to calculate solutions for the first and second sections of the pipe, a way must be found to approximate these values.

In figure fig. 7.1 a schematic outline of the process outlined above. By using this process for solving the pipelaying problem, only a full Finite Element simulation has to be run for the part with contact with the stinger and the other parts can be approximated by other methods.

7.2 Further research

In this section some points of interest are listed which could be a starting point for further research.

Conservative contact methods The Augmented Barrier and Augmented Lagrangian methods work too well for dynamic problems, making any solutions non-realistic because of the loss of energy conservation. It would be advisable to look into contact methods (apart from the Penalty method) which preserve the energy in the system.

Two articles seem to be a promising basis for designing new contact methods which work with a Lagrangian parameter and are also conserving energy. Armero [24] proposes a Penalty regularization method, which conserves energy in the dynamical system during contact and releases the energy back into the system once the contact has ended. A more recent contribution by Ayyad [25] provides a numerical study with a discretization scheme based on the Finite Element method and gives error estimates for the solutions.

Further simplifications Two main strategies for simplification have been presented in this thesis, namely the approximation of the middle section of the pipe which is not under influence of contact restrictions, and approximating the contact point of the dynamic solution at the seabed with a static solution in that region.

Possibly more ways can be found to calculate parts of the solution without actually simulating the entire solution with the Finite Element method with contact enforced. It is mainly important to determine the parts which are of interest. In case of the pipe: is the contact point important, the region where contact is made, the curvature of the pipe or even the entire solution (the deflection of the pipe at every place and at every point in time).

Usability of the static solution A simplification is proposed in Section 6.6 by using the static solution instead of simulating the entire dynamic solution in order to determine the point of contact with the seabed. However, this simplification has only been verified under certain mild conditions. It would be good to verify quantitatively under which conditions the assumption can be made that the static solution is good enough for finding the contact point.

Even if the static solution may be used to approximate the dynamic point of contact, it may be analyzed how susceptible even the static solution is to vibrations and fluctuations in the boundary conditions, and how much these vibrations influence the point of contact.

Finally it must be noted that in general the static solution including contact cannot be determined analytically, as was sometimes possible in this research. If no analytic static solution (and its point of contact) is available, a method must be determined to approximate the point of contact well from a numeric solution.

Differently shaped contact surfaces The shape of the contact surface has been varied in order to simulate the surface of the stinger or a sloped seabed. At the moment only a basic Finite Element implementation has been used of the linear model for the pipe. Once the contact methods have been extended to a non-linear method such as the co-rotational method, some things must be investigated further. Among them are the possible shapes of the contact surface which provide good solutions, the usability of static solutions on a specific surface shape (see previous paragraph).

Furthermore, if a non-linear model is used for the pipe and the solution domain is more than one dimensional, the pipe can also 'roll' sideways over the seabed. Depending on the shape of the surface, this behaviour must be analyzed to determine if it is relevant to the problem. The model involving friction during contact may need to be extended for this scenario.

Hit on stinger A deeper analysis of contact with the stinger can be useful to determine the characteristics of contact during large movements of the ship. The pipe will most likely hit the stinger in some specific places depending on the movement. Depending on the findings, the location, size and nature of the Finite Elements may be adjusted on the stinger in order to provide the best accuracy and performance while keeping the required behaviour of the solution.

Bibliography

- [1] Demeter G. Fertis. *Nonlinear Structural Engineering*. Springer, 2006.
- [2] Ferdinand P. Beer, Jr. E. Russell Johnston, John T. Dewolf, and David F. Mazurek. *Mechanics of Materials, 10th edition*. Pearson, 2017.
- [3] Leonard Mierovitch. *Fundamentals of Vibrations*. McGraw Hill, July 2000.
- [4] Simon J.A. Malham. *An introduction to Lagrangian and Hamiltonian mechanics, Lecture Notes*. Heriot-Watt University, Mathematics Department, 2016.
- [5] E. Minguzzi. Rayleigh's dissipation function at work. *European Journal of Physics*, 36(3), February 2015.
- [6] Gertjan Kloosterman. *Contact Methods in Finite Element Simulations*. Ponsen & Looijen, Wageningen, December 2002.
- [7] Juan C. Simo, Peter Wriggers, and Robert L. Taylor. A perturbed lagrangian formulation for the finite element solution of contact problems. *Computer Methods in Applied Mechanics and Engineering*, 50(2):163 – 180, August 1985.
- [8] Xuefeng Li. Augmented lagrangian methods for numerical solutions to higher order differential equations. *Journal of Applied Mathematics and Physics*, 5(2):239–251, 2017.
- [9] Sang-Un Kim and Chang-Ock Lee. Accurate surface reconstruction in 3d using two-dimensional parallel cross sections. *Journal of Mathematical Imaging and Vision*, 53(2):182–195, October 2015.
- [10] Chongchao Huang and Song Wang. A power penalty approach to a nonlinear complementarity problem. *Operations Research Letters*, 38(1):72–76, January 2010.
- [11] J. van Kan, A. Segal, and F. Vermolen. *Numerical Methods in Scientific Computing*. Delft Academic Press, VSSD, November 2014.
- [12] Eric Sonnendrücker and Ahmed Ratnani. Advanced finite element methods, lecture notes, 2016.
- [13] NamHo Kim. Finite element analysis of beams and frames. University of Florida, EML 5526, 2014.
- [14] Louie L. Yaw. 2D Corotational beam formulation. Walla Walla University, 2009.
- [15] J.W. Craighead. *A Mathematical Discussion of Corotational Finite Element Modeling*. Canadian theses. Queen's University (Kingston, Ont.). Department of Mathematics and Statistics, 2011.
- [16] T. K. Caughey and M. E. J. O'Kelly. Classical normal modes in damped linear dynamic systems. *Journal of Applied Mechanics*, 32(3):583–588, September 1965.
- [17] John H. Mathews and Kurtis K. Fink. *Numerical Methods Using Matlab, 4th edition*. Prentice-Hall Inc, January 2004.
- [18] Basem S. Attili. The Hilber-Hughes-Taylor- α (HHT- α) method compared with an implicit Runge-Kutta for second-order systems. *International Journal of Computer Mathematics*, 87(8):1755–1767, 2010.

- [19] M.A. Dokainish. A survey of direct time-integration methods in computational structural dynamics. *Computers & Structures - COMPUT STRUCT*, 32:1371–1386, January 1989.
- [20] Henri P. Gavin. Numerical integration in structural dynamics, Lecture notes CEE 541. Duke University, Department of Civil & Environmental Engineering, 2016.
- [21] P.F. Gou and K. Panah K. Analytical solution for beam with time dependent boundary conditions versus response spectrum. *International Conference on Nuclear Engineering*, 2001.
- [22] G. A. Baker, Jr. The Theory and Application of the Padé Approximant Method. In *Advances in Theoretical Physics, Volume 1*, page 1, 1965.
- [23] Sakshat Virtual Labs. Free vibration of a cantilever beam (continuous system). <http://iitg.vlab.co.in/?sub=62&brch=175&sim=1080&cnt=1>, 2011.
- [24] Francisco Armero and Eva Petőcz. Formulation and analysis of conserving algorithms for frictionless dynamic contact/impact problems. *Computer Methods in Applied Mechanics and Engineering*, 158(3):269 – 300, 1998.
- [25] Y. Ayyad, M. Barboteu, and J.R. Fernández. A frictionless viscoelastodynamic contact problem with energy consistent properties: Numerical analysis and computational aspects. *Computer Methods in Applied Mechanics and Engineering*, 198(5):669 – 679, 2009.

Nomenclature

'	Derivative in spatial direction
α	Parameter for HHT- α method
α_1, α_2	Coefficients to determine Rayleigh damping
β	Parameter for Newmark- β method
'	Derivative in spatial direction
η	Weiging constant for the λ update step
γ	Parameter for Newmark- β method
\hat{L}	Point of contact for analytic static solution
$\lambda(x)$	Langrangian parameter
$\lambda_0(x)$	Initial value for $\lambda(x)$
μ	Mass per unit length [kg/m]
∇	Differential operator
∂	A partial derivative
$\mathcal{L}(t, x, y, \dot{y}, y', \ddot{y}, y'')$	The Lagrangian operator
ψ	Updating factor for p
τ	Time integration step size
ς_j	Weights for Gauss-Legendre interpolation
$\vartheta_{t,k}$	$y'_t(x_k)$
$\Xi(d_N(y))$	Penalty functional for a contact method
C	Damping matrix
c_c	Damping constant for damping on contact
c_d	Damping constant
$d_N(y)$	The gap [m]
E	The elastic modulus [N/m^2]
e_k	Element k for the Finite Element method

NOMENCLATURE

F_c	Drag force for damping on contact [N]
F_d	Damping force [N]
I	The second moment of inertia [m ⁴]
$J_n(y)$	The energy functional of the beam which is minimized for y
K	Stiffness matrix
L_k	Length of element k
M	Mass matrix
N	Number of elements
$N(\xi_k)$	Matrix of basis function values at ξ_k
p	Penalty parameter
$p_0(x)$	Initial value for p
P_k	Permutation matrix for element k
q_k	Finite Element state vector
$q_{t,k}$	Coefficients at two ends of element k
s	Laplace frequency parameter
t	Time, temporal variable [s]
$U_i(s; x)$	Laplace input or output function
$w(t, x)$	The distributed load on the beam [N]
x	Location, spatial variable [m]
$Y(s; x)$	Laplace transformed $y(t, x)$
$y(t, x)$	The deflection of the beam at time t at position x [m]
$y_t(x)$	$y(t, x)$
$y_{t,k}$	$y_t(x_k) = y(t, x_k)$

Appendix A

Appendix

A.1 Hermite shape functions

The Hermite shape functions are determined by solving the static problem (2.13) with boundary conditions

$$y(0) = y_0, \quad y'(0) = \vartheta_0, \quad y(L) = y_L, \quad y'(L) = \vartheta_L. \quad (\text{A.1})$$

Then the basis functions are determined as the four functions ϕ_1 , ϕ_2 , ϕ_3 and ϕ_4 which satisfy the values of the boundary conditions

$$\begin{aligned} \phi_1: \quad & y_0 = 1, \vartheta_0 = 0, y_L = 0, \vartheta_L = 0, \\ \phi_2: \quad & y_0 = 0, \vartheta_0 = 1, y_L = 0, \vartheta_L = 0, \\ \phi_3: \quad & y_0 = 0, \vartheta_0 = 0, y_L = 1, \vartheta_L = 0, \\ \phi_4: \quad & y_0 = 0, \vartheta_0 = 0, y_L = 0, \vartheta_L = 1. \end{aligned} \quad (\text{A.2})$$

A.2 Analytic solutions of dynamic Euler Bernoulli equation

The problem in (2.9) is solved with $w = 0$ and $c_d = 0$ and homogeneous boundary conditions given by

$$y(t, 0) = 0, \quad y'(t, 0) = 0, \quad (\text{A.3})$$

$$EIy''(t, L) = 0, \quad (\text{A.4})$$

$$EIy'''(t, L) = 0 \quad (\text{A.5})$$

and initial conditions $y(0, x) = y_0(x)$ and $\dot{y}(0, x) = v_0(x)$. We make the *ansatz* (assumption) that the solution $y(t, x) = X(x)T(t)$. This technique is called *separation of variables*. This gives a new form of (2.9) after deriving the separated variables, namely

$$EIX''''(x)T(t) + \mu X(x)\ddot{T}(t) = 0 \quad (\text{A.6})$$

which is satisfied if and only if

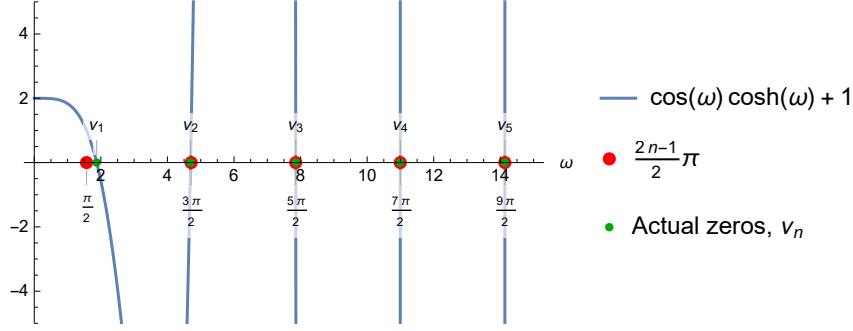
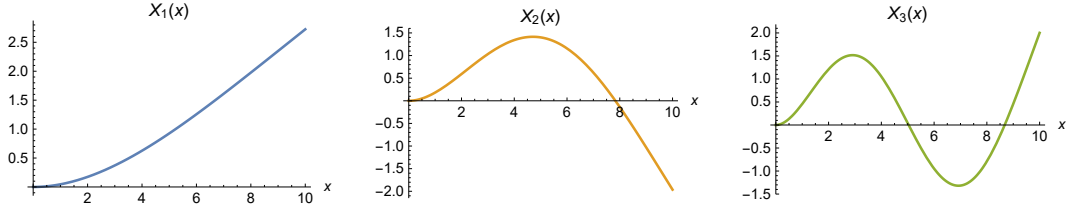
$$X''''(x) = \nu^4 X(x), \quad \ddot{T}(t) = -\omega^2 T(t) \quad (\text{A.7})$$

are satisfied and $\omega^2 = (EI/\mu)\nu^4$. This gives that

$$X(x) = A \sin(\nu x) + B \cos(\nu x) + C \sinh(\nu x) + D \cosh(\nu x), \quad T(t) = F \sin(\omega t) + G \cos(\omega t). \quad (\text{A.8})$$

Using (A.8), the boundary conditions (A.3) impose that $A = -C$ and $B = -D$, which gives the expression

$$y(t, x) = (F \sin(\omega t) + G \cos(\omega t)) \left(A (\sin(\nu x) - \sinh(\nu x)) + B (\cos(\nu x) - \cosh(\nu x)) \right). \quad (\text{A.9})$$


FIGURE A.1: The zeros of (A.10) compared to $\frac{2n-1}{2}\pi$.

FIGURE A.2: First three modes $X_n(x)$ of the analytical solution.

After solving the equations for (A.4) the constant B is resolved to $B = (\sin(vL) + \sinh(vL))/(\cos(vL) + \cosh(vL))$. Finally, to impose the final boundary condition (A.5), the frequencies of the lengthwise terms (v) are determined as solutions of

$$\cosh(v_n L) \cos(v_n L) + 1 = 0 \quad (\text{A.10})$$

with solutions v_n for $n \in \mathbb{N}_+ = \{1, 2, 3, \dots\}$. This means that the expression for $y(t, x)$ becomes an infinite sum, built up of the different vibration modes in the solution. The first numerical values of $v_n L$ are

$$v_1 L \approx 1.8751 \quad v_2 L \approx 4.69409 \quad v_3 L \approx 7.85476 \quad v_4 L \approx 10.9955. \quad (\text{A.11})$$

These values become very close to $(2n-1)/2\pi$ for higher values of n . A comparison is given in fig. A.1. A visualization of the first three modes $X_n(x)$ can be found in fig. A.2.

This gives the final expression for the clamped-free-end beam problem as

$$y(t, x) = \sum_{n=1}^{\infty} A_n (F_n \sin(\omega_n t) + G_n \cos(\omega_n t)) \left((\sin(v_n x) - \sinh(v_n x)) + B (\cos(v_n x) - \cosh(v_n x)) \right) \quad (\text{A.12})$$

with $\omega_n^2 = (EI/\mu)v_n^4$ and where the constants $A_n F_n$ and $A_n G_n$ are determined by the initial conditions $y_0(x)$ and $v_0(x)$. Because $\sin(\omega_n t)$ and $\cos(\omega_n t)$ are orthogonal for all n and to each other, the series can be seen as a Fourier series and the coefficients $A_n F_n$ and $A_n G_n$ can be found using

$$A_n G_n = \frac{\int_0^L y_0(x) X_n(x) dx}{\int_0^L X_n(x)^2 dx}, \quad A_n F_n = \frac{1}{\omega_n} \frac{\int_0^L v_0(x) X_n(x) dx}{\int_0^L X_n(x)^2 dx}. \quad (\text{A.13})$$

A.3 Discrete Fourier Transform for eigenvalues

In Section 6.1.1 the frequency of the dynamic solution is compared with the analytical values for a specific problem. The eigenvalues of the dynamical system are determined by finding the eigenvalues of the corresponding Finite Element matrices. In this section another method is used to determine the same eigenvalues of the system, however in a different way than by using the Finite Element matrices.

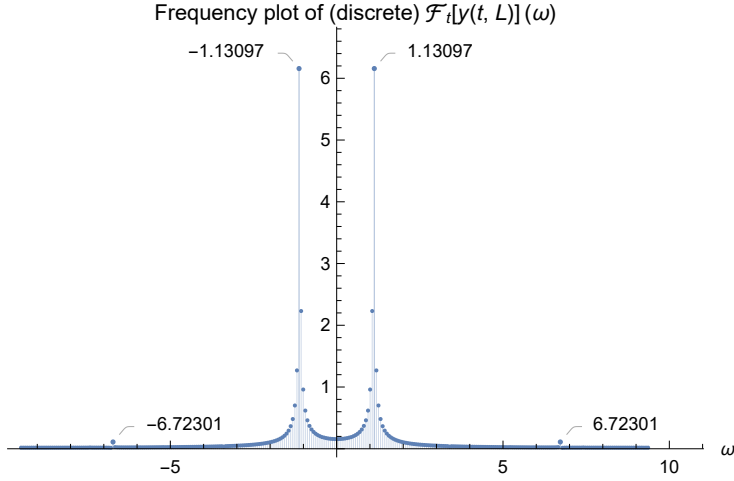


FIGURE A.3: Discrete Fourier transform of the FEM solution at $x = L$, using a sample rate of 3 samples per second and a sample time of 100 seconds. The frequencies of the first and second mode of the solution are labelled.

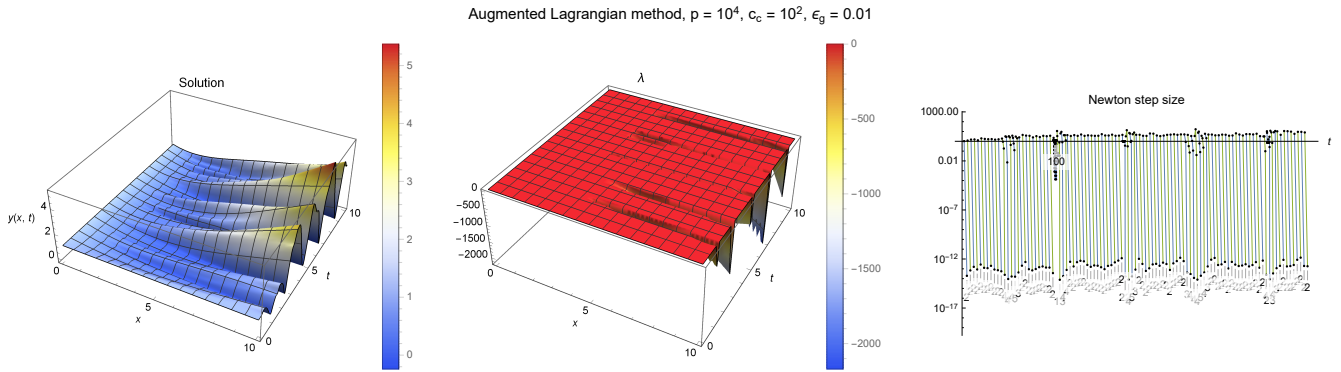


FIGURE A.4: Damped solution on contact using the Augmented Lagrangian method with $p = 10^4$, $c_c = 10^2$ and $\epsilon_g = 0.01$.

A simulation of the dynamical system has been performed of the problem given in (2.11) with (6.3) as boundary conditions. The constants $EI = 10^4$ [Nm²], $\mu = 10$ [kg/m], $L = 10$ [m], $\tau = 0.1$ [s/step] and $\alpha = 0$, and $N = 8$ elements have been used. Then the numerical solution at $x = L$ is taken, which makes a sinusoidal movement over time. Of this time series a discrete fourier transform is taken which from which the first eigenvalues of the system are determined.

In fig. A.3 a discrete Fourier transform of the FEM solution at $x = L$ can be found, which has been created using a linear interpolation (order 1), a sample rate of 3 per second and a sample time of 100 seconds. The first and second mode can be seen clearly. The values of the first two modes that can be observed in the FEM solution show that it is very close to the analytical solution of the mode frequencies.

Because a time step of $\tau = 0.1$ has been used for time integration, it is logical that solution frequencies of higher than 10 Hz (corresponding to $\omega = 20\pi$) cannot be found in the FEM solution. Furthermore, if τ is set to 0.02, a tiny peak can be found in the discrete Fourier transform plot around $\omega \approx 19.2$ which corresponds to ω_3 in the analytical solution (not displayed in the figure).

A.4 Damping on contact

In Section 6.4.2 the results of damping on contact are shown for a simulation run with the Penalty method for enforcing contact. The same simulation has been run using the Augmented Lagrangian and Augmented Barrier contact methods. However the results are not useful because of the bad solutions. Still, for completeness, the results are shown in fig. A.4 (Augmented Lagrangian) and fig. A.5 (Augmented Barrier).

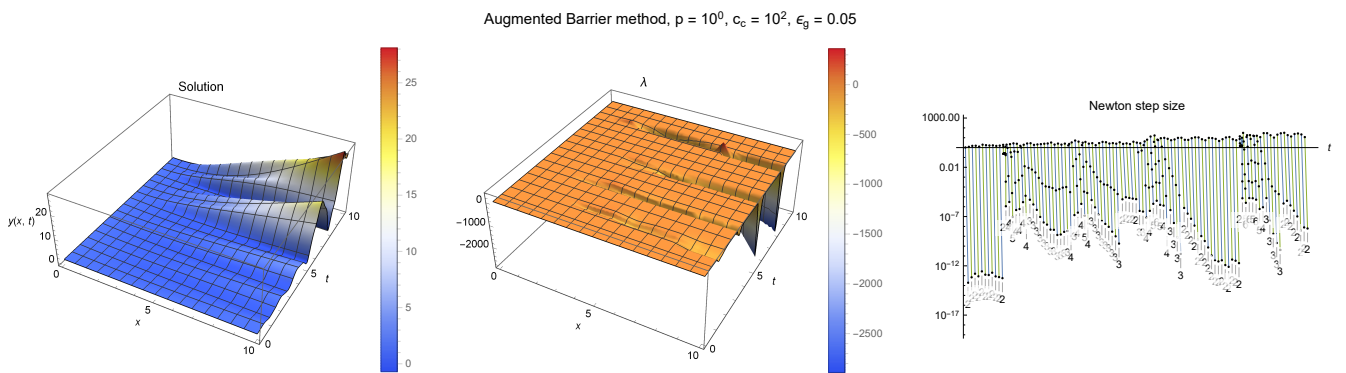


FIGURE A.5: Damped solution on contact using Augmented Barrier method with $p = 10^0$, $c_c = 10^2$ and $\epsilon_g = 0.01$.